

1 **LA-ICPMS U-Pb geochronology of detrital zircon grains from the Coconino,**
2 **Moenkopi, and Chinle Formations in the Petrified Forest National Park (Arizona)**

3
4
5 George Gehrels¹, Dominique Giesler¹, Paul Olsen², Dennis Kent³, Adam Marsh⁴, William Parker⁴,
6 Cornelia Rasmussen⁵, Roland Mundil⁵, Randall Irmis⁶, John Geissman⁷, and Christopher Lepre³

7 ¹Department of Geosciences, University of Arizona, Tucson AZ 85721, USA

8 ²Lamont-Doherty Earth Observatory of Columbia University, Palisades, NY 10964, USA

9 ³Earth and Planetary Sciences, Rutgers University, Piscataway, NJ 08854, USA

10 ⁴Petrified Forest National Park, Petrified Forest, AZ 86028, USA

11 ⁵Berkeley Geochronology Center, 2455 Ridge Rd., Berkeley CA 94709, USA

12 ⁶Natural History Museum of Utah and Department of Geology & Geophysics,
13 University of Utah, Salt Lake City, UT 84108, USA

14 ⁷Department of Geosciences, University of Texas at Dallas, Richardson, TX 75080, USA

15
16
17
18
19
20 *Correspondence to George Gehrels (ggehrels@gmail.com)*

21 *28 May draft; re-submitted to Geochronology*

22 *(revised to accommodate review and AE comments)*

24 **ABSTRACT**

25 U-Pb geochronology was conducted by Laser Ablation-Inductively Coupled Plasma Mass
26 Spectrometry (LA-ICPMS) on 7,175 detrital zircon grains from twenty-nine samples from the
27 Coconino Sandstone, Moenkopi Formation, and Chinle Formation. These samples were
28 recovered from ~520 m of drill core that was acquired during the Colorado Plateau Coring
29 Project (CPCP), located in Petrified Forest National Park (Arizona).

30 A sample from the lower Permian Coconino Sandstone yields a broad distribution of
31 Proterozoic and Paleozoic ages that are consistent with derivation from the Appalachian and
32 Ouachita orogens, with little input from local basement or Ancestral Rocky Mountain sources.
33 Four samples from the Holbrook Member of the Moenkopi Formation yield a different set of
34 Precambrian and Paleozoic age groups, indicating derivation from the Ouachita orogen, the
35 East Mexico Arc, and the Permo-Triassic arc built along the Cordilleran margin.

36 Twenty-three samples from the Chinle Formation contain variable proportions of Proterozoic
37 and Paleozoic zircon grains, but are dominated by Late Triassic grains. LA-ICPMS ages of these
38 grains belong to five main groups that correspond to the Mesa Redondo Member, Blue Mesa
39 Member and lower part of the Sonsela Member, upper part of the Sonsela Member, middle
40 part of the Petrified Forest Member, and upper part of the Petrified Forest Member. The ages
41 of pre-Triassic grains also correspond to these chronostratigraphic units, and are interpreted to
42 reflect varying contributions from the Appalachian orogen to the east, Ouachita orogen to the
43 southeast, Precambrian basement exposed in the Ancestral Mogollon Highlands to the south,
44 East Mexico arc, and Permian-Triassic arc built along the southern Cordilleran margin. Triassic
45 grains in each chronostratigraphic unit also have distinct U and Th concentrations, which are
46 interpreted to reflect temporal changes in the chemistry of arc magmatism.

47 Comparison of our LA-ICPMS ages with available CA-TIMS ages and new magnetostratigraphic
48 data provides new insights into the depositional history of the Chinle Formation, as well as
49 methods utilized to determine depositional ages of fluvial strata. For parts of the Chinle
50 Formation that are dominated by fine-grained clastic strata (e.g. mudstone and siltstone), such
51 as the Blue Mesa Member and Petrified Forest Member, all three chronometers agree (to
52 within ~1 m.y.), and robust depositional chronologies have been determined. In contrast, for
53 stratigraphic intervals dominated by coarse-grained clastic strata (e.g., sandstone), such as
54 most of the Sonsela Member, the three chronologic records disagree due to recycling of older
55 zircon grains and variable dilution of syn-depositional-age grains. This results in LA-ICPMS ages
56 that significantly pre-date deposition, and CA-TIMS ages that range between the other two
57 chronometers. These complications challenge attempts to establish a well-defined
58 chronostratigraphic age model for the Chinle Formation

59 **1. INTRODUCTION**

60 Triassic strata of the Colorado Plateau and environs provide rich and geographically extensive
61 records of environmental and biotic change during a critical period of Earth history, as well as
62 the transition from passive- to convergent-margin tectonism along the North American
63 Cordillera (e.g., Parker and Martz, 2011; Olsen et al., 2011). As demonstrated by Riggs et al.
64 (1996, 2003, 2012, 2013, 2016), Dickinson and Gehrels (2008), Irmis et al. (2011), Ramezani et
65 al. (2011, 2014), Atchley et al. (2013), Nordt et al. (2015), Kent et al. (2018, 2019), Olsen et al.
66 (2018, 2019), Marsh et al. (2019), and Rasmussen et al. (2020), Chinle Formation strata have
67 the potential to record the timing of these changes in great detail given their several-hundred-
68 meter thickness, abundance of near-depositional-age zircon grains, and recoverable
69 paleomagnetic reversal stratigraphy.

70 In an effort to further develop this record, ~520 m of continuous core was collected from
71 Triassic and underlying Permian strata at Petrified Forest National Park (PEFO), which is located
72 on the southern Colorado Plateau of northern Arizona (Fig. 1; (35.085933° N, 109.795500° W,
73 WGS84 datum). The objectives and primary findings of this project have been described by
74 Olsen et al. (2018, 2019), Kent et al. (2018, 2019), and Rasmussen et al. (2020), and numerous
75 related studies are currently in progress. This contribution to the project reports U-Pb
76 geochronologic analyses of detrital zircon grains that were extracted from twenty-nine samples
77 from this core (CPCP-PFNP13-1A). Analyses were conducted by laser ablation-inductively
78 coupled mass spectrometry (LA-ICPMS), with between 36 and 490 grains analyzed per sample
79 (total of 7,175 analyses). Grains were chosen for analysis by random selection in an effort to
80 provide unbiased information about provenance. Fortunately, a significant number of near-
81 depositional-age grains were recovered from many samples in the Chinle Formation, which
82 provides opportunities to also determine robust maximum depositional ages. This report
83 explores variations in both provenance and maximum depositional age of strata intersected in
84 the CPCP-PFNP13-1A core, and the implications for Permian-Triassic environmental and biotic
85 transformations and the tectonic evolution of southwestern North America.

86 **2. STRATA ENCOUNTERED IN THE PETRIFIED FOREST NATIONAL PARK DRILL CORE**

87 The lowest stratigraphic horizon encountered consists of quartz arenite belonging to the
88 Coconino Sandstone (Fig. 2). This unit belongs to regionally extensive erg deposits of early
89 Permian (Leonardian) age (Blakey et al., 1988; Lawton et al., 2015; Dickinson, 2018).

90 Overlying strata of the Coconino Sandstone are tabular, thin to thick-bedded, reddish
91 mudstone, siltstone, and sandstone layers of the Lower-Middle Triassic Moenkopi Formation. In
92 the PEFO region, the Moenkopi Formation consists of thin-bedded reddish siltstone with
93 interlayered sandstone and mudstone. Lower, finer-grained strata are assigned to the Wupatki
94 Member and Moqui Member, and upper sandstone-rich horizons dominate the Holbrook
95 Member. The base is a regional unconformity, the TR-1 unconformity of Pipiringos and
96 O'Sullivan (1978), along which strata of the lower Permian Toroweap Formation and Kaibab

97 Formation have been removed. Strata of the Moenkopi Formation are interpreted to have
98 accumulated on a northwest-sloping coastal plain, with thinner fluvial strata to the southeast
99 and thicker marginal marine strata to the northwest (Dickinson, 2018). The Moenkopi
100 Formation basin was bounded by residual uplifts of the Ancestral Rocky Mountains to the
101 northeast and highlands of the Ouachita orogen to the southeast. Highlands developed within
102 early phases of the Cordilleran magmatic arc may have existed to the southwest.

103 Strata of the Moenkopi Formation are overlain unconformably [Tr-3 unconformity of Pippingos
104 and O'Sullivan (1978)] by the Chinle Formation (Fig. 2). The transition is marked in most areas
105 by the Shinarump Conglomerate, which consists of cobbles of chert, quartzite, limestone and
106 subordinate felsic volcanic rocks. Riggs et al. (2012) have determined U-Pb ages of 232-224 Ma
107 on volcanic cobbles in the Shinarump Conglomerate. The Shinarump Conglomerate is
108 interpreted to correlate with finer-grained strata of the Mesa Redondo Member (Irmis et al.,
109 2011; Martz et al., 2012, 2017; Riggs et al., 2016). Strata of the Shinarump Conglomerate and
110 Mesa Redondo Member are interpreted to have accumulated in paleovalleys that were carved
111 into underlying strata. Strikingly variegated, strongly pedogenically modified, red, purple, and
112 yellow strata in the core are assigned to the Mesa Redondo Member given the lack of
113 conglomerate. Strata of the Mesa Redondo Member in outcrop have yielded U-Pb (zircon) ages
114 of ~227.6 Ma (Atchley et al., 2013) and ~225.2 Ma (Ramezani et al., 2011).

115 Gradationally overlying the Mesa Redondo Member are strata of the Blue Mesa Member,
116 which consist of purplish to gray and red bentonitic mudstone with sandstone beds that are
117 generally 0.5 m in thickness (Woody, 2006). Blue Mesa Member mudstones are pervasively
118 pedogenically modified in the core. These strata are interpreted to have accumulated primarily
119 as overbank deposits within a mixed-load meandering river system (Martz and Parker, 2010).
120 Previously reported U-Pb (ID-TIMS or CA-TIMS) ages from outcrop of the Blue Mesa Member
121 range from ~223 Ma to ~218 Ma (Heckert et al., 2009; Ramezani et al., 2011; Irmis et al., 2011;
122 Atchley et al., 2013; Rasmussen et al., 2020).

123 Strata of the Blue Mesa Member are overlain by sandstone-rich and conglomerate-bearing
124 strata of the Sonsela Member. Lucas (1993) and Heckert and Lucas (2002) refer to the base of
125 the Sonsela Member as a regionally significant unconformity, although this interpretation has
126 been questioned by Woody (2006) and Martz and Parker (2010) given that conglomeratic
127 sandstone of the Sonsela is interbedded with mudstone of the Blue Mesa Member. Martz and
128 Parker (2010) suggest that the transition from the Blue Mesa Member to the Sonsela Member
129 marks a change in depositional regime (from mainly overbank deposits to bedload-dominated
130 channel deposits) but does not mark a significant hiatus in deposition.

131 The Sonsela Member consists predominantly of sandstone with lesser mudstone and local
132 conglomerate. Sandstone beds are variable in thickness, have significant lateral extent, and
133 exhibit cut-and-fill structure (Woody, 2006). Conglomerate (with abundant volcanic clasts) is
134 common within the sandstone beds. Five units have been recognized, a lower sandstone
135 interval (Camp Butte beds), a lower-middle unit with abundant mudstone (Lot's Wife beds), a

136 middle sandstone and conglomerate unit (Jasper Forest/Rainbow Forest bed), a middle-upper
137 unit with pedogenic carbonate and abundant mudstone (Jim Camp Wash beds), and an upper
138 sandstone unit (Martha's Butte beds) (Martz and Parker, 2010). The five units are gradational,
139 with the main variation being the abundance of mudstone in two of the middle units. A reddish
140 siliceous horizon of uncertain regional extent has been recognized within the middle of the
141 upper mudstone-rich unit in the CPCP-PFNP13-1A core. Similar horizons within other exposures
142 of the Sonsela Member are marked by a significant die-off of the conifers that characterize
143 Petrified Forest National Park (Creber and Ash, 1990), a turn-over of the vertebrate fauna
144 (Parker and Martz, 2009, 2011), and perhaps a significant change in flora and paleoclimate
145 (Reichgelt et al., 2013; Nordt et al., 2015; Baranyi et al., 2017). U-Pb (CA-TIMS/zircon) ages from
146 the Sonsela Member range from ~220 to ~214 Ma (Ramezani et al., 2011; Marsh et al., 2019;
147 Rasmussen et al., 2020) from below the siliceous horizon and from ~214 to ~213 Ma (Ramezani
148 et al., 2011; Nordt et al., 2015; Kent et al., 2018; Rasmussen et al., 2020) from above.

149 Overlying the conglomeratic sandstones of the Sonsela Member is a purplish mudstone that
150 marks the base of the Petrified Forest Member (Fig. 2). This member consists of red and purple
151 mudstone with abundant paleosols and pedogenic carbonate nodules, with local conglomeratic
152 sandstone beds that formed in bedload-dominated streams. Near the top of the unit is the
153 Black Forest bed, which consists of limestone-pebble conglomerate and reworked andesitic tuff
154 (Ash, 1992). Zircon grains from the Black Forest bed have yielded U-Pb (ID-TIMS or CA-TIMS)
155 ages of ~213 Ma to ~210 Ma (Riggs et al., 2003; Heckert et al., 2009; Ramezani et al., 2011; Kent
156 et al., 2018; Rasmussen et al., 2020).

157 **3. SAMPLED HORIZONS**

158 We analyzed detrital zircon grains from twenty-nine samples collected from the Permian and
159 Triassic strata described above. Samples include one from the Coconino Sandstone, five from
160 the Moenkopi Formation (one that may be from the Wupatki Member and four from the
161 Holbrook Member), and twenty-three from the Chinle Formation (one from the Mesa Redondo
162 Member, three from the Blue Mesa Member, twelve from the Sonsela Member, and seven
163 from the Petrified Forest Member). Approximate stratigraphic positions of the samples are
164 shown on Figure 2, lithic characteristics are described in DR Table 1, and images of the sampled
165 material (both core and thin sections) are presented in Appendix 1. Each sample consisted of 20
166 cm (for sandstone) to 30 cm (for mudstone-siltstone) of $\frac{1}{4}$ sections of the core.

167 **4. ANALYTICAL AND INTERPRETIVE METHODS**

168 Zircon mineral separation was performed at the Arizona LaserChron Center
169 (www.laserchron.org) using methods modified from those outlined by Gehrels (2000), Gehrels
170 et al. (2008), and Gehrels and Pecha (2014) because of the small size of all samples and the
171 abundance of clay minerals in many samples. The process included using a hand-crusher to
172 break the samples apart, a gold pan for initial density separation, and an ultrasonic disruptor
173 (Hoke et al., 2014) to separate zircon crystals from clay mineral grains. Magnetic separation was

174 performed with a Frantz Isodynamic separator, followed by density separation using methylene
175 iodide.

176 Zircon grains greater than 60 μm in size were enclosed in 1-inch epoxy mounts along with
177 fragments of zircon standards SL (primary) and FC-1 and R33 (secondary). Mounts were
178 polished approximately 5-10 μm deep to expose the internal structure of the grains but retain
179 as much material as possible for subsequent CA-TIMS analysis. Imaging was performed with a
180 backscatter electron detector system (BSE) using a Hitachi S3400 scanning electron microscope
181 (SEM) to ensure analysis of zircon and to avoid inclusions and fractures. Mounts were cleaned
182 with 1% HCl and 1% HNO₃ prior to isotopic analysis.

183 U-Pb isotopic analyses were conducted by LA-ICPMS using a Teledyne/Photon Machines
184 Analyte G2 laser connected to a Thermo Element2 mass spectrometer. Analyses utilized a 20
185 μm diameter laser beam fired at 7 hz for 15 seconds, resulting in 10-12 μm deep pits. Details of
186 the analytical methods are reported in DR Table 2.

187 U-Pb ages are calculated with an in-house data-reduction routine (E2agecalc) following
188 methods of Pullen et al. (2018). Analyses of zircon grains from our samples are reported in DR
189 Table 3, with results filtered for discordance (using cutoffs of 80% and 105% concordance),
190 precision (10%), and common Pb (>600 cps counts of 204). Following the recommendations of
191 Horstwood et al. (2016), uncertainties for individual analyses include only internal (random or
192 measurement) uncertainty contributions, whereas uncertainties of pooled ages contain both
193 internal and external (systematic) contributions.

194 Detrital age distributions are displayed and analyzed with normalized probability density plots,
195 which are based on the individual ages and measured uncertainties from each sample.
196 Provenance interpretations are based on the main clusters of ages, with less emphasis on ages
197 that do not belong to clusters given the possibility that they are unreliable due to Pb loss,
198 inheritance, analysis of inclusions, high common Pb, or unusual Pb/U fractionation due to
199 ablation along fractures (Gehrels, 2014).

200 Analysis of provenance is conducted by comparison with age distributions from five likely
201 source regions for Permian-Triassic strata of the Colorado Plateau, which include the
202 Appalachian orogen, the Ouachita orogen, local basement rocks of southwestern Laurentia, the
203 East Mexico arc, and the Permian-Triassic magmatic arc developed along the Cordilleran margin
204 of southwestern North America (Fig. 1; Dickinson, 2018). The age distributions for these regions
205 include data from: (1) upper Paleozoic strata of the Appalachian foreland basin (Thomas et al.,
206 2017) and Illinois and Forest City basins (Kissock et al., 2018), (2) upper Paleozoic strata of the
207 Delaware (Xie et al., 2018), Fort Worth (Absalem et al., 2018), and Marathon (Thomas et al.,
208 2019) basins, (3) lower Paleozoic strata of the Grand Canyon (Gehrels et al., 2011) and
209 Cordilleran passive margin strata in southern California and northern Sonora (Gehrels and
210 Pecha, 2014), (4) Permian and Triassic strata of the Barranca and El Antimonio Formations of
211 Sonora (Gonzalez-Leon et al., 2009; Gehrels and Pecha, 2014), Jura-Cretaceous strata of the

212 Great Valley (DeGraaff-Surpless et al., 2002; Surpless et al., 2006; Wright and Wyld, 2007),
213 Permian-Triassic igneous rocks in California (Chen and Moore, 1982; Miller et al., 1995; Tobisch
214 et al., 2000; Barth and Wooden, 2006, 2011, 2013; Saleeby and Dunne, 2015), and (5) Mesozoic
215 strata that accumulated adjacent to the East Mexico arc (Ortega-Flores et al., 2014). Age
216 distributions for these five regions are presented in Figure 3.

217 Comparisons of age distributions are quantified using several different statistical measures that
218 examine the degree to which age distributions contain similar proportions of similar age
219 groups. Five metrics used in this study include the cross-correlation coefficient, values of
220 similarity and likeness, and the Kolmogorov-Smirnov (K-S) D values and Kuiper V values. The
221 statistical basis as well as strengths and limitations of each of these metrics are summarized by
222 Saylor and Sundell (2016), Wissink et al. (2018), and Vermeesch (2018a). Results from these
223 comparisons are presented in DR Table 4. The interpretations offered below are based on
224 cross-correlation coefficients, although all five metrics yield similar results. Comparisons are
225 also presented visually through the use of multidimensional scaling (MDS) diagrams
226 (Vermeesch, 2013; Wissink et al., 2018), which provide a 2-dimensional representation of the
227 differences between multiple age distributions. MDS analyses are also based on cross-
228 correlation coefficients.

229 Maximum depositional ages are determined from estimates of the age of the youngest
230 distinct cluster of three or more overlapping ages (Dickinson and Gehrels, 2009; Gehrels, 2014).
231 The age of this cluster is estimated using four different methods, each of which have strengths
232 and limitations. Complications with these methods arise from (1) the need to make
233 unconstrained decisions about which analyses to include or exclude from consideration, (2) the
234 evidence from complicated PDP age distributions and high (>1.0) MSWD values that the
235 youngest clusters for most samples contain multiple age populations, (3) the evidence that
236 dates in some clusters have been compromised by Pb loss, and (4) issues of statistical
237 robustness for some methods (Vermeesch, 2018b). Following are short descriptions of the four
238 methods:

- 239 • Age of the youngest peak on a probability density plot (PDP). This method is advantageous
240 because no decisions are made about which analyses are included/excluded, but it has the
241 disadvantage that no uncertainty is reported for the peak age.
- 242 • Weighted Mean age and uncertainty of the youngest cluster. This method calculates the
243 average age of a cluster by weighting each analysis according to the inverse-square of its
244 uncertainty. The reported uncertainty relates to the mean age (e.g., standard error of the
245 mean), not the age distribution of constituent analyses (e.g., standard deviation). An
246 advantage of this method is that it also yields a Mean Square of the Weighted Deviates
247 (MSWD), which is an indication of the degree to which the ages belong to a single
248 population (values of ~1 or less indicate a single population). A disadvantage of this method
249 is that the investigator must decide which ages are included in the calculation, which leads
250 to the possibility of subjective bias. In this study, clusters include the main set of continuous

251 ages, with boundaries selected at the youngest and oldest gap in ages. This calculation is
252 available from the Weighted Mean function in Isoplot (Ludwig, 2008).

- 253 • Tuffzirc age and uncertainty of the youngest cluster. This method uses the age extractor
254 function in Isoplot (Ludwig, 2008), which identifies the largest cluster of ages that overlap to
255 an acceptable degree (probability-of-fit > 0.05), reports the median value as the most likely
256 age, and uses the range of included ages to calculate an asymmetric uncertainty. The
257 reported uncertainty refers to the median value (not the range of constituent analyses).
258 Excluded ages are interpreted to pre-date the selected cluster (if older), or to be
259 compromised by Pb loss (if younger). This method is advantageous in that no subjective
260 decisions are made about including/excluding ages.
- 261 • Maximum Likelihood age and uncertainty. This method uses a maximum likelihood analysis
262 to determine the gaussian distribution that best fits the youngest cluster. The reported
263 uncertainty refers to the most likely value (not the range of constituent analyses). This
264 method is advantageous in that no subjective decisions are made about including/excluding
265 ages. It is available from the Unmix function of Isoplot (Ludwig, 2008).

266

267 The results of these calculations are presented in DR Tables 3 and 6.

268 DR Table 6 also reports the age and uncertainty of the youngest analysis from each sample. This
269 youngest age does not provide a reliable maximum depositional age given that the youngest
270 age of a distribution will always be younger than the true age due to analytical uncertainty
271 (Gehrels, 2014). For example, as described by Coutts et al. (2019), consider the analytical data
272 from a population of zircon grains that have exactly the same true age. Because of analytical
273 uncertainty, the measured ages of half of the analyses will be younger than the true age, and
274 half will be older, and the youngest age will be significantly younger than the mean (true) age.
275 Ironically, the more grains analyzed, the greater the inaccuracy of this youngest age!

276 In addition to this statistical bias, the youngest single age will be even farther from the mean
277 (true) age if it has been compromised by Pb loss (e.g., Andersen et al., 2019). We report these
278 youngest ages because they provide important information about the possibility that analyses
279 included in the youngest cluster have also experienced Pb loss. DR Table 6 accordingly reports
280 this youngest age (and uncertainty), as well as information about its U concentration, the
281 average U concentration of the youngest cluster of ages, and whether the youngest age belongs
282 to the youngest cluster or is an outlier. U concentration is important because Pb loss is
283 commonly correlated with the degree of radiation damage, which is a function of U
284 concentration (and age).

285 A second test of the likelihood that analyses belonging to the youngest cluster have
286 experienced Pb loss is provided by a plot of U concentration versus age for analyses belonging
287 to the youngest cluster. Such plots are shown for every sample in DR Table 3, and whether a
288 correlation exists is indicated in DR Table 6.

289 Also included in DR Table 6 are the preferred age and uncertainty for each sample. The
290 preferred age is based on the average of the four age estimates determined by peak age,
291 weighted mean, Tuffzirc, and Unmix analyses. The uncertainty of this preferred age is based on
292 the average of the uncertainty from each method, and is shown with both internal-only
293 uncertainties and with combined internal and external uncertainties.

294 The average precision of individual analyses reported herein is 2.3% (2σ) for $^{206}\text{Pb}^*/^{238}\text{U}$ dates
295 and 2.6% for $^{206}\text{Pb}^*/^{207}\text{Pb}^*$ dates. For pooled ages, calculated as described above, the average
296 precision is 0.52% (2σ) including only internal uncertainties and 0.98% (2σ) including both
297 internal and external sources of uncertainty. The accuracy of our analyses can be estimated
298 from the age of the secondary standards that were analyzed with each set of unknowns. As
299 reported in DR Table 7 and shown on Figure 4, sets of $^{206}\text{Pb}^*/^{238}\text{U}$ dates for FC-1 are offset
300 between +0.25% and -0.45% from the reported $^{206}\text{Pb}^*/^{238}\text{U}$ date of 1099.9 Ma (Paces and
301 Miller, 1993), with an average offset for all 1,065 analyses of +0.03%. For R33, offsets range
302 from +0.85% to -0.95% from the assumed age of 419.3 Ma (Black et al., 2004), with an average
303 offset for all 291 ages of -0.23%. MSWD values for the sets of FC-1 and R33 ages are 0.95 and
304 0.92 (respectively) – this demonstrates that reported uncertainties for individual analyses are
305 accurate, and that MSWD values for sets of unknown ages are reliable indicators of the
306 existence of multiple age components.

307 Interpretation of our ages relative to the Geologic Time Scale is based on the August 2018
308 version of the International Chronostratigraphic Chart (Cohen et al., 2013).

309 U-Pb geochronology by LA-ICPMS also provides U concentrations and U/Th values for each
310 analysis, which can be used as a geochemical fingerprint of detrital zircon grains (e.g., Gehrels
311 et al., 2006, 2008; Riggs et al., 2012, 2016). This information is accordingly reported for each
312 analysis in DR Table 3, and for each set of analyses in DR Table 6.

313 **5. U-Pb GEOCHRONOLOGIC RESULTS**

314 Results of our U-Pb geochronologic analyses are described below, keyed to the age
315 distributions for individual samples that are shown on Figures 5, 6, and 7. Figure 8 presents age
316 distributions for combined sets of samples. Age distributions from all of the samples are
317 compared statistically in DR Table 4 using the five metrics described above, and MDS plots are
318 shown in Figure 9.

319 We note that Rasmussen et al. (2020) have reported a subset of the LA-ICPMS ages presented
320 herein. The ages reported in their study are for the grains selected for CA-TIMS analysis, which
321 in most cases are among the youngest grains in each of our samples (as documented in
322 Appendix 2). This strategy was followed assuming that these grains represent the youngest age
323 components in each sample, and accordingly provide the most useful maximum depositional
324 ages. The individual dates reported in the two studies are identical, but, given the selection
325 process noted above, the pooled ages reported by Rasmussen et al. (2020) are consistently

326 younger than the pooled ages reported herein. A comparison of the results of the two studies is
327 summarized in Appendix 2. The discussions below are based on the full set of ages from each
328 sample.

329 Sample numbers are registered to the CPCP core (CPCP-PFNP13-1A) by the number of the core
330 run and segment (e.g., our sample number 383-2 is from CPCP-PFNP13-1A-383Y-2, which
331 specifies that the material is from run 383, segment 2). The part of each segment that was
332 collected for geochronologic analysis is specified in DR Table 1.

333 **5.1 Coconino Sandstone**

334 Our sample from quartz arenite of the lower Permian (Leonardian) Coconino Sandstone
335 (sample 390-1) yielded 285 acceptable ages (DR Table 3; Figure 4). Most grains belong to two
336 broad age groups of ~2.0-1.0 Ga and ~640-295 Ma. Individual age peaks are at 2712, 1898,
337 1746, 1646, 1497, 1432, 1347, 1162, 1038, 667, 612, 590, 552, 476, 430, 419, 391, 374, 355,
338 341, and 300 Ma.

339 **5.2 Moenkopi Formation**

340 Five samples from the Lower-Middle Triassic Moenkopi Formation have been analyzed (Fig. 2).
341 The lowest sample (383-2) is assigned to the Wupatki Member based on the red-brown
342 laminated mudstone to fine-grained sandstone lithology (Fig. 2; Table DR 1). The age
343 distribution from this sample is very similar to that found in underlying upper Paleozoic strata,
344 with two dominant age groups from ~2.2 Ga to 1.0 Ga and from ~680 Ma to 250 Ma (Fig. 5).
345 Although the preferred interpretation for this sample is that it belongs to the lowest part of the
346 Moenkopi Formation, an alternative is that the sample is late Paleozoic in age, and perhaps
347 correlative with fine-grained clastic strata (e.g., the Toroweap Formation) that regionally overlie
348 the Coconino Sandstone. In an effort to provide a comparison with underlying and overlying
349 strata, the results from this sample are shown on Figures 5 and 6. Additional studies of the
350 sampled horizon are needed to resolve whether this sample belongs to the Moenkopi
351 Formation or underlying upper Paleozoic strata.

352 The upper four samples (349-3, 335-1, 327-2, and 319-2) are all from sandstone, siltstone, and
353 mudstone of the Holbrook Member. These samples yield generally similar age distributions
354 (average CCC of 0.24; DR Table 4), with significant proportions of ~1.42 Ga, 650-510 Ma, 290-
355 270 Ma, and 250-235 Ma ages (Fig. 6). With ages from all four Moenkopi Formation samples
356 combined, PDP peak ages are 1420, 594, 543, 285, and 250 Ma (Fig. 8). As shown in Figures 9B
357 and 9C, age distributions from the lower two samples (349-3 and 335-1) and upper two samples
358 (327-2 and 319-2) form two distinct groups. These clusters are also apparent from CCC values of
359 0.83 and 0.24 for the lower and upper samples (respectively), in comparison with a low average
360 value (0.08) for comparison of the two sets with each other (DR Table 4).

361 **5.3 Chinle Formation**

362 Twenty-three samples from the Mesa Redondo Member, Blue Mesa Member, Sonsela Member,
363 and Petrified Forest Member of the Chinle Formation have been analyzed (Fig. 2). Results from
364 each member are described separately below.

365 **5.4 Mesa Redondo Member**

366 One sample of sandstone from the Mesa Redondo Member (305-2) yields dominant age groups
367 of ~2.0-1.6 Ga, 1.44 Ga, 1.1-1.0 Ga, 750-500 Ma, and 450-300 Ma, and 290-220 Ma (Fig. 7), with
368 PDP peak ages of 1443, 1036, 618, 412, 323, 248, and 223 Ma. As reported in DR Table 4 and
369 shown on Figure 9C, the >240 Ma ages in this samples resemble ages in the underlying
370 Moenkopi Formation and Coconino Sandstone.

371 **5.5 Blue Mesa Member**

372 Three samples (297-2, 287-2, 261-1) of siltstone and mudstone from the Blue Mesa Member
373 yield very similar results, with nearly identical <240 Ma ages and small but varying proportions
374 of ~1.64 Ga, 1.44 Ga, 1.1-1.0 Ga, 650-500 Ma, and 440-240 Ma ages (Figures 7 and 8). Both
375 <240 Ma ages (Fig. 9A) and >240 Ma ages (Fig. 9C) differ from those in underlying strata of the
376 Mesa Redondo Member. Between 56% and 89% of the grains analyzed from these samples
377 yield ages between 232 and 210 Ma, with PDP peak ages of 221-220 Ma (Fig. 7; DR Table 6).
378 With all three samples combined, 62% of the ages are <240 Ma, and PDP peak ages are 1630,
379 1440, and 220 Ma (Fig. 8).

380 **5.6 Sonsela Member**

381 Twelve samples (243-3 to 158-2) from the Sonsela Member yield two different sets of age
382 distributions (Figures 7, 8, and 9; DR Table 3). The lower six samples (243-3 to 196-3), all
383 consisting of sandstone and subordinate siltstone (DR Table 1), yield small numbers of
384 Precambrian grains that are mostly ~1.65 and 1.44 Ga, with few ~1.1-1.0 Ga grains. These
385 samples yield between 53% and 79% ages <240 Ma, with most ages between 234 and 208 Ma,
386 and PDP peak ages of 221-218 Ma (Fig. 7). With ages from all six samples combined, 68% of the
387 grains are <240 Ma, and PDP peak ages are 1650, 1445, 1084, and 219 Ma (Fig. 8). Comparison
388 of age distributions (Figures 7 and 8), CCC values (DR Table 4), and MDS patterns (Fig. 9)
389 suggests that the <240 Ma ages in these strata are indistinguishable from <240 Ma ages in
390 underlying Blue Mesa strata, whereas >240 Ma ages in the two sets of samples are less similar
391 due to the variability of ages from the three Blue Mesa Member samples. Ages that are >240
392 Ma in these strata have even less similarity to ages from the Mesa Redondo Member,
393 Moenkopi Formation, and Coconino Sandstone (Fig. 9; DR Table 4).

394 The upper six samples from the Sonsela Member (195-2 to 158-2) consist mainly of sandstone
395 and subordinate siltstone (DR Table 1). All six samples yield a subordinate but consistent
396 proportion of Precambrian ages that are mostly ~1.43 and 1.1-1.0 Ga, with few 1.65 Ga grains
397 (Fig. 7). Grains with ages of <240 Ma comprise between 39% and 77% of the grains analyzed.
398 These ages are somewhat younger than in lower Sonsela Member samples, with PDP peak ages

399 of 217-214 Ma. With all six samples combined, 50% of the grains are <240 Ma, and PDP peak
400 ages are 1643, 1434, 1082, 256, and 215 Ma (Fig. 8).

401 Statistical analysis (MDS patterns in Figure 9 and CCC values in DR Table 4) shows that the <240
402 Ma ages in upper and lower Sonsela Member strata are significantly different, whereas >240
403 Ma ages are less distinct. Exceptions to this are >240 Ma ages in sample 243-3 (lower Sonsela
404 Member), which resemble equivalent ages in strata of the upper Sonsela Member (Fig. 9C), and
405 <240 Ma ages in sample 196-3, which share characteristics with strata of both the upper and
406 lower Sonsela Member (Fig. 9A). Ages from strata of the upper Sonsela Member show even less
407 overlap with ages from strata of the Blue Mesa Member and underlying units (Fig. 9 and DR
408 Table 4).

409 **5.7 Petrified Forest Member**

410 Seven samples (131-2 to 52-2) from the Petrified Forest Member were collected mainly from
411 claystone, mudstone, siltstone, and fine-grained sandstone, with only the lowest sample (131-
412 2) consisting of coarse-grained sandstone. The upper six fine-grained samples yield between
413 17% and 72% <240 Ma ages that are significantly younger than in underlying strata, with PDP
414 peak ages between 212 and 209 Ma. Ages that are >240 Ma in these samples differ from
415 equivalent ages in strata of the Blue Mesa Member and Sonsela Member, but overlap to
416 varying degrees with ages in strata of the Mesa Redondo Member, Moenkopi Formation, and
417 Coconino Sandstone (Fig. 9C; DR Table 4). With the six samples combined, 35% of the grains are
418 <240 Ma, and PDP peak ages are 1636, 1430, 1032, 629, 379, 287, and 209 Ma (Fig. 8). The
419 lowest sample (131-2), consisting of coarse-grained sandstone, differs from the other Petrified
420 Forest Member samples, with an age peak of 221 Ma, and a greater proportion (68%) of >240
421 Ma ages (Fig. 7). The <240 Ma ages are very similar to equivalent ages in strata of the lower
422 Sonsela Member (Fig. 9A; CCC=0.97), whereas >240 Ma ages are more similar to ages in the
423 upper Sonsela Member (CCC=0.72) than in the lower Sonsela Member (CCC=0.59) (Fig. 9C).

424 **5.8 Summary of Chinle results**

425 The patterns of LA-ICPMS ages described above suggest that the studied part of the Chinle
426 Formation comprises four different units, each of which has a distinct chronologic signature for
427 both <240 Ma and >240 Ma ages (Fig. 8). These chronostratigraphic units correspond to the
428 Mesa Redondo Member, Blue Mesa Member and lower part of the Sonsela Member, upper
429 part of the Sonsela Member, and Petrified Forest Member.

430 **6. U AND Th GEOCHEMISTRY OF CHINLE ZIRCON GRAINS**

431 In an effort to evaluate whether the Triassic zircon grains from the four chronostratigraphic
432 units also have distinct chemical signatures [following Riggs et al. (2012, 2016)], Figure 10
433 summarizes the U concentrations and U/Th values for Triassic zircon grains analyzed from each
434 unit. The patterns exhibited in these plots suggest that (1) zircon grains from the Mesa
435 Redondo Member are significantly different from zircon grains in overlying strata, (2) grains in

436 strata of the Blue Mesa Member and lower Sonsela Member differ from grains in overlying
437 strata of the upper Sonsela Member and Petrified Forest Member, and (3) grains in strata of the
438 upper Sonsela Member and Petrified Forest Member have distinctive and slightly different
439 bimodal patterns. Plots showing U concentrations and U/Th values for individual samples are
440 included in DR Table 3.

441 **7. PROVENANCE INTERPRETATIONS**

442 Detrital zircon geochronology has previously been used to reconstruct the provenance of
443 Permian and Triassic strata of the Colorado Plateau by Riggs et al. (1996, 2003, 2012, 2013,
444 2016), Dickinson and Gehrels (2003, 2008), Gehrels et al. (2011), Lawton et al. (2015), and
445 Marsh et al. (2019). The results of most of these geochronologic studies, and a large number of
446 stratigraphically based analyses, have recently been summarized by Dickinson (2018). The
447 following sections compare our new results with this existing information.

448 The following comparisons are based in part on qualitative comparison of age distributions of
449 the strata that we have analyzed and of age distributions from five potential source areas
450 (summarized on Figure 3). As described by Gehrels (2000), such comparisons focus on the
451 degree to which two age distributions contain similar proportions of similar ages. Comparisons
452 are also based on the results of statistical analyses (DR Table 4) that compare our results with
453 the age distributions of possible source areas, and on graphic displays of these comparisons
454 using MDS plots (Fig. 9).

455 **7.1 Coconino Sandstone**

456 Lawton et al. (2015) and Dickinson (2018) suggest that lower Permian strata of the Colorado
457 Plateau comprise a regional blanket of eolian strata that was shed predominantly from the
458 Appalachian and/or Ouachita orogens, with increasing input in northern regions from local
459 basement rocks exposed in the Uncompahgre or Ute Uplift (Fig. 1). These interpretations are
460 supported by the age distributions shown on Figures 5 and 11, with southern strata (Coconino,
461 Cedar Mesa, and White Rim sandstones) forming a distinct group dominated by
462 Appalachian/Ouachita detritus, and northern strata (Castle Valley and Cutler strata) forming a
463 separate group with increasing proportions of ca 1.44 Ga grains. The age distribution from our
464 Coconino Sandstone sample (390-1) fits well with other strata from the southern Colorado
465 Plateau in having abundant 1.2-1.0 and 670-300 Ma grains and a low proportion of ~1.44 Ga
466 grains (Figures 5 and 11; DR Table 4).

467 **7.2 Moenkopi Formation**

468 As summarized on Figure 6, the detrital zircon ages from our four Holbrook Member samples
469 are generally similar to ages from a Holbrook Member sandstone reported by Dickinson and
470 Gehrels (2008). Dominant >300 Ma age groups and interpreted source terranes include ~1.44
471 Ga and subordinate ~2.0-1.6 Ga grains derived from Laurentian Precambrian basement and
472 ~670-300 Ma grains derived from Ouachita/Gondwana sources. Based on comparison with

473 detrital zircon ages from strata that accumulated in proximity to the East Mexico and southern
474 Cordilleran arcs (Fig. 3), 300-260 Ma grains (PDP peak ages of 285, 284, 265, 260, and 279) are
475 interpreted to have been shed from the East Mexico arc (peak age of 284 Ma), whereas 260-
476 230 Ma grains (peak ages of 250, 248, 228, 245, and 239 Ma) were likely shed from Early-
477 Middle Triassic parts of the Cordilleran magmatic arc in California and northwestern Mexico
478 (peak ages of 243, 236, and 226 Ma) (Fig. 3). Statistical analyses (DR Table 4) suggest nearly
479 equal contributions from the Ouachita orogen, local basement rocks, and the East Mexico arc.

480 More detailed analysis of the age distributions (Fig. 6) and MDS patterns (Fig. 9) suggest that
481 the lower two samples (349-3 and 335-1) [plus sample CP8 of Dickinson and Gehrels (2008)] are
482 dominated by ~1.44 Ga and ~285 Ma grains, whereas the upper two samples (327-2 and 319-2)
483 are dominated by ~620-590 Ma and ~250-230 Ma grains. The age distributions (Fig. 6) and
484 comparison metrics (Fig. 9; DR Table 4) suggest that the lower samples were shed mainly from
485 local basement rocks (CCC=0.30) and the East Mexico arc (CCC=0.22), whereas the upper
486 samples were shed largely from the Ouachita orogen (CCC=0.23).

487 **7.3 Chinle Formation**

488 Our results from detrital zircon grains recovered from strata of the Chinle Formation are
489 consistent with the provenance and paleogeographic reconstructions offered by Riggs et al.
490 (1996, 2003, 2012, 2013, 2016), Dickinson (2018), and Marsh et al. (2019). Given the observed
491 age distributions (Fig. 7) and the location of our study site relative to Late Triassic
492 paleogeographic and paleotectonic features of southwestern North America (Fig. 12), likely
493 sources for pre-Triassic grains include rocks exposed in the Ouachita orogen to the southeast
494 and the Ancestral Mogollon highlands to the south and southwest. Given the abundance of ash
495 layers, bentonitic mudstone, and near-depositional-age zircon grains in strata of the Chinle
496 Formation, and the existence of arc-related plutons and volcanic rocks of Triassic age in Sonora
497 and southern California (Barth and Wooden, 2006, 2011, 2013; Saleeby and Dunne, 2015; Riggs
498 et al., 2016), Stewart et al. (1986), Riggs et al. (2012, 2016), Dickinson (2018), Marsh et al.
499 (2016), and many other researchers conclude that Triassic grains in Chinle strata were derived
500 from the active arc built along the southern Cordilleran margin. The occurrence in fore-arc and
501 back-arc strata of very similar distributions of ages (Fig. 3) is inconsistent with interpretations
502 (e.g., Hildebrand, 2009, 2013) that the early Mesozoic arc was located far from southwestern
503 North America.

504 Although our data are entirely consistent with the provenance interpretations outlined above,
505 the density of our sampling and the large number of analyses from most samples provide
506 opportunities to reconstruct temporal changes in Triassic provenance in greater detail, and with
507 the benefit of statistical analyses to quantify conclusions. Following are interpretations based
508 on strata belonging to each of the different members of the Chinle Formation.

509 **7.4 Mesa Redondo Member**

510 The provenance of strata belonging to the Mesa Redondo Member is similar to that of the
511 underlying Moenkopi Formation, with our sample (305-2) containing abundant ~640-300 Ma
512 grains derived from Ouachita/Gondwana sources as well as ~290-260 Ma grains derived from
513 the East Mexico arc (Fig. 8). Statistical analysis confirms higher similarity of >240 Ma grains with
514 Ouachita sources (0.58) than with Appalachian (0.35) or local basement (0.15) sources (DR
515 Table 4). This sample also yields a significant proportion of Triassic ages that approximate the
516 depositional age for these strata (Fig. 7). These young grains, with a PDP age peak of 223 Ma,
517 are interpreted to have been transported primarily by aeolian processes from the active
518 magmatic arc to the west (Fig. 12). Statistical analysis demonstrates that the Triassic ages in
519 these samples are significantly different from ages in overlying strata (Fig. 9A) and that the
520 >240 Ma ages are similar to those in strata of the Petrified Forest Member (Fig. 9C).

521 **7.5 Blue Mesa Member**

522 Our three samples from strata of the Blue Mesa Member yield a large proportion of Triassic
523 zircon grains (Figures 7 and 8) that were derived from the active Cordilleran magmatic arc to
524 the west (Fig. 12), and a small proportion of pre-240 Ma grains that were shed from local
525 basement rocks and the Ouachita and/or Appalachian orogens (Fig. 8). Statistical analysis
526 confirms that the Triassic ages in all these samples are quite similar (Fig. 9A), whereas the age
527 distributions of >240 Ma grains in the three samples are more variable (Fig. 9C; DR Table 4).

528 **7.6 Lower Sonsela member**

529 The lower six samples from the Sonsela Member yield a large proportion of Triassic grains
530 derived from the Cordilleran magmatic arc, and fewer ages derived from local basement rocks
531 and Ouachita/Gondwana sources (Figures 7 and 8). Distinctive among the older grains is a
532 significant proportion of ~1.44 Ga grains that most likely signal increased input from the
533 Ancestral Mogollon highlands to the southwest (Marsh et al., 2019) (Fig. 12). MDS analysis
534 demonstrates that the <240 Ma and >240 Ma ages in these samples are quite similar, with the
535 only significant difference being the larger number of ~1.1 Ga grains in sample 243-3 (Figures 7
536 and 9C).

537 **7.7 Upper Sonsela Member**

538 The upper six samples from the Sonsela Member reveal a continued low contribution from the
539 Ouachita orogen, and a significant increase in the proportion of ~1.08 Ga and 260-240 Ma
540 grains (Figures 7 and 8). The ~260-240 Ma grains were likely derived from Permian-Early Triassic
541 igneous rocks along the southern Cordilleran margin (Saleeby and Dunne, 2015; Riggs et al.,
542 2016), exposed in the Ancestral Mogollon Highlands (Fig. 12). The prominent ~1.44 and 1.08 Ga
543 grains in these samples may also have been shed from highland sources to the south and
544 southwest. Triassic grains in these samples record a slightly younger (230 to 204 Ma, peak age
545 of 215 Ma) phase of magmatism along the Cordilleran margin. Significant changes in both <240
546 Ma and >240 Ma ages occur between samples 196-3 and 195-2 (Figure 7). MDS analysis
547 demonstrates that patterns of both <240 Ma and >240 Ma ages are consistent among the six

548 upper Sonsela Member samples, but are distinct from ages in all other parts of the Chinle
549 Formation (Figures 7 and 9).

550 **7.8 Petrified Forest Member**

551 Strata of the Petrified Forest Member record an important shift in provenance, with
552 significantly greater detrital input from the East Mexico arc (~287 Ma) and the Ouachita orogen
553 (~640-300 Ma), and a broader range of >1.0 Ga basement sources (Figures 7 and 8). Triassic
554 grains in these strata are also significantly younger, with ages of 228 to 200 Ma (peak age of
555 209 Ma).

556 An exception to these patterns is recorded by ages from the coarse-grained sandstone of
557 sample 131-2, which has Precambrian grains that are mainly ~1.1-1.0 and 1.44 Ga (like upper
558 Sonsela Member; Fig. 9B), and Triassic grains that are ~221 Ma (like strata of the lower Sonsela
559 Member and Blue Mesa Member; Fig. 9A). This lower Petrified Forest Member sample is
560 interpreted to have been reworked mainly from lateral equivalents of underlying strata of the
561 Sonsela Member and Blue Mesa Member, with little or no input from the active arc to the west.
562 MDS analysis shows that sample 116-1 contains a mix of these older reworked grains and the
563 younger grains present in overlying strata (Fig. 9A).

564 **8. MAXIMUM DEPOSITIONAL AGES**

565 The depositional age of Triassic strata on the Colorado Plateau is of considerable interest
566 because of the rich faunal and paleoclimatic records preserved within the Moenkopi Formation
567 and Chinle Formation, and as the zircon-based geochronological framework for the early
568 Mesozoic when coupled with paleomagnetic polarity stratigraphy and astrochronology (Olsen
569 et al., 2018, 2019; Kent et al., 2018, 2019; Rasmussen et al., 2020). There accordingly have been
570 many prior attempts to determine the depositional age of these strata by dating igneous zircon
571 grains in ash beds or volcanic cobbles and detrital zircon grains in clastic strata (e.g., Riggs et al.,
572 1996, 2003, 2012, 2013, 2016; Heckert et al., 2009; Dickinson and Gehrels, 2009; Irmis et al.,
573 2011; Ramezani et al., 2011, 2014; Atchley et al., 2013; Nordt et al., 2015). As part the Colorado
574 Plateau Coring Project, Kent et al. (2018) and Rasmussen et al. (2020) report the results of CA-
575 TIMS analyses on many of the same samples reported herein. All of the available CA-TIMS ages,
576 and the preferred age models of Kent et al. (2019) and Rasmussen et al. (2020), are shown on
577 Figure 13.

578 Maximum depositional ages (MDA's) have been calculated from the LA-ICPMS ages using four
579 different methods (described above), with results presented in DR Tables 3 and 6 and shown
580 graphically on Figure 13. In the following discussion we assume that the average of the ages
581 and uncertainties calculated using these four different methods yields the most reliable
582 maximum depositional age available from our LA-ICPMS data. These preferred ages are
583 reported in DR Table 6, shown on Figure 13, and described below with 2σ uncertainties
584 incorporating only internal contributions (for inter-sample comparison) and incorporating both

585 internal and external uncertainty contributions (for comparison with ages from other studies)
586 (e.g., $224.4 \pm 2.0/2.7$ Ma).

587 The possibility that a maximum depositional age has been compromised by Pb loss is evaluated
588 by determining whether there is a correlation between U concentration and age. One criterion
589 is whether the youngest single age has higher U concentration than the average of the
590 youngest cluster – if yes than the youngest analysis (and perhaps other analyses within the
591 youngest cluster) may have experienced Pb loss. A second criterion is whether analyses within
592 the youngest cluster display an inverse correlation between U concentration and age – if yes,
593 then the higher U and younger analyses within the cluster may have experienced Pb loss.
594 Rasmussen et al. (2020) document Pb loss in zircon grains from several of our samples by
595 showing that CA-TIMS ages are commonly older than LA-ICPMS ages from the same crystals.

596 **8.1 Coconino Sandstone**

597 Our analyses do not provide a useful maximum depositional age for strata of the Coconino
598 Sandstone (sample 390-1) because few late Paleozoic ages were recovered from this sample.

599 **8.2 Holbrook Formation of the Moenkopi Formation**

600 Of our four samples from the Holbrook Member of the Moenkopi Formation, three yield
601 preferred MDA's that young upward from $249.5 (\pm 1.6/2.5)$ Ma to $248.4 (\pm 2.0/2.8)$ Ma to 245.7
602 $(\pm 1.9/2.7)$ Ma (DR Table 6). These MDA's are consistent with the inferred Early-Middle Triassic
603 age of the strata and the corresponding ~ 251 - 237 Ma range for Early and Middle Triassic time
604 on the Geologic Time Scale (Cohen et al., 2013). All three samples show patterns of U
605 concentration that suggest the possibility of Pb loss (DR Table 6).

606 **8.3 Mesa Redondo Member of the Chinle Formation**

607 Our one sample (305-2) from strata of the Mesa Redondo Member yields a preferred MDA of
608 $223.3 \pm 1.3/2.2$ Ma (DR Table 6). A low MSWD value (0.5) suggests that all ages belong to the
609 same age population, and patterns of U concentration do not indicate the presence of Pb loss.
610 This MDA overlaps with CA-TIMS ages of ~ 224.7 - 221.7 Ma from the same sample but is older
611 than the preferred single-grain age of ~ 221.7 Ma (Rasmussen et al., 2020). The LA-ICPMS MDA
612 of $223.3 \pm 1.3/2.2$ is significantly younger than CA-TIMS ages of ~ 225.2 Ma (Ramezani et al.,
613 2011) and ~ 227.6 (Atchley et al., 2013) from outcrop samples of the Mesa Redondo Member.

614 **8.4 Blue Mesa Member of the Chinle Formation**

615 Our three samples (297-2, 287-2, 261-1) from strata of the Blue Mesa Member yield preferred
616 MDA's of $220.6 \pm 0.6/2.1$, $220.2 \pm 1.3/2.2$, and $220.7 \pm 1.3/1.9$ Ma (DR Table 6). All samples
617 yield MSWD values >1.0 (average of 2.4), which documents the presence of multiple age
618 populations. Patterns of U concentration suggest the presence of Pb loss in all three samples.
619 As shown on Figure 13, these ages are similar to most CA-TIMS ages from strata of the Blue
620 Mesa Member. From lower strata, our ages are slightly younger than a CA-TIMS age of ~ 221.8

621 Ma [from sample 297-2; Rasmussen et al. (2020)], indistinguishable from a CA-TIMS age of
622 ~ 220.5 Ma [from sample 287-2; Rasmussen et al. (2020)]. From upper strata, our age is similar
623 to a CA-TIMS age from outcrop of ~ 220.1 Ma (Atchley et al., 2013) but significantly younger
624 than a CA-TIMS age of ~ 223.0 Ma (Ramezani et al., 2011), also from outcrop.

625 **8.5 Lower part of the Sonsela Member**

626 Our six samples from the lower part of the Sonsela Member (243-3 to 196-3) yield preferred
627 MDA's of $220.3 \pm 0.9/1.8$ Ma (sample 243-3), $220.6 \pm 0.5/1.8$ Ma (sample 227-3), $220.5 \pm$
628 $0.6/1.6$ Ma (sample 215-2), $220.9 \pm 0.7/2.3$ Ma (sample 210-1), and $220.6 \pm 0.6/1.7$ Ma (sample
629 201-1). The sixth, uppermost sample (196-3) yields younger ages with a preferred MDA of 218.2
630 $\pm 0.7/1.6$ Ma. MSWD values for these samples are all high (average of 2.6), which demonstrates
631 the presence of multiple age components.

632 As shown on Figure 13, these MDA's are 1-3 m.y. older than most CA-TIMS ages from
633 equivalent strata. From oldest to youngest, the CA-TIMS ages include ~ 220.1 Ma [from outcrop;
634 Atchley et al. (2013)] from near the base, through ~ 218.8 Ma [sample 243-3; Rasmussen et al.
635 (2020)], ~ 217.7 Ma [sample 227-3; Rasmussen et al. (2020)], ~ 219.3 Ma [from outcrop;
636 Ramezani et al. (2011)], ~ 217.8 Ma [sample 215-2; Rasmussen et al. (2020)], ~ 218.0 Ma [from
637 outcrop; Ramezani et al. (2011)], and ~ 215.7 Ma and 214.4 Ma [samples 201-1 and 196-3;
638 Rasmussen et al. (2020)] at the top. The LA-ICPMS-based MDA's ages are also older than a
639 ~ 216.6 Ma MDA determined on LA-ICPMS ages from an outcrop sample of sandstone in the
640 middle part of the lower Sonsela Member, exposed ~ 132 km north of the CPCP core site (Marsh
641 et al., 2019).

642 **8.6 Upper part of the Sonsela Member**

643 The lower five samples from the upper Sonsela Member yield similar preferred MDA's of 215.4
644 $\pm 1.1/2.2$ Ma (sample 195-2), $216.5 \pm 0.7/1.9$ Ma (sample 188-2), $216.1 \pm 0.9/2.1$ Ma (sample
645 182-1), $215.1 \pm 0.8/1.9$ Ma (sample 177-1), and $216.6 \pm 1.0/2.0$ Ma (sample 169-1). An upper
646 sample yields a younger MDA of $213.8 \pm 0.6/2.1$ Ma (sample 158-2). All samples yield MSWD
647 values greater than 1.0 (average of 2.6), demonstrating the presence of multiple age
648 components. Most samples have patterns of U concentration that suggest the possibility of Pb
649 loss. The lower five MDA's are 2-3 m.y. older than CA-TIMS ages from equivalent strata, which
650 include outcrop ages of ~ 213.9 (Ramezani et al., 2011), ~ 213.6 Ma (Nordt et al., 2015), and
651 ~ 213.1 Ma (Ramezani et al., 2011), and CPCP core ages of ~ 214.0 Ma [samples 182-1 and 177-1;
652 Rasmussen et al. (2020)]. A CA-TIMS age of ~ 213.5 Ma for the upper sample [158-2; Rasmussen
653 et al. (2020)] is nearly identical to our age determination.

654 **8.7 Petrified Forest Member**

655 Our seven samples from the Petrified Forest Member yield three sets of preferred MDA's. The
656 lowest unit (sample 131-2) yields an MDA of $221.5 \pm 0.6/2.1$ Ma, which is significantly older
657 than MDA's in adjacent strata. Four samples near the middle of the unit yield similar preferred

658 MDA's of $211.5 \pm 3.1/3.4$ Ma (sample 116-1), $211.6 \pm 1.7/2.5$ Ma (sample 104-3), $211.2 \pm$
659 $1.2/1.9$ Ma (sample 92-2), and $211.7 \pm 1.0/2.0$ Ma (sample 84-2). These MDA's are very similar
660 to an ID-TIMS age of ~ 211.9 Ma (Irmis et al., 2011) from equivalent strata in outcrop. Two
661 upper samples, from the Black Forest bed, yield preferred MDA's of $209.6 \pm 3.0/3.4$ Ma (sample
662 66-1) and $209.8 \pm 0.5/1.6$ Ma (sample 52-2). These MDA's are similar to CA-TIMS ages of ~ 210.2
663 Ma from core [sample 52-2; Rasmussen et al. (2020)] and ~ 209.9 Ma from outcrop (Ramezani
664 et al., 2011), but are significantly younger than outcrop-based ID-TIMS ages of ~ 211.0 Ma
665 (Heckert et al., 2009) and ~ 213.0 Ma (Riggs et al., 2003). Most of our samples yield MSWD
666 values greater than 1.0 (average of 1.5), suggesting the presence of multiple age components,
667 and have patterns of U concentration that suggest the presence of Pb loss.

668 **9. COMPARISON OF LA-ICPMS, CA-TIMS, AND MAGNETOSTRATIGRAPHIC CONSTRAINTS ON** 669 **DEPOSITIONAL AGE OF CHINLE FORMATION STRATA**

670 Our preferred maximum depositional ages for strata of the Chinle Formation range from ~ 223.3 to
671 ~ 209.6 Ma, which is similar to the ~ 227.6 to ~ 209.9 Ma range of CA-TIMS ages (Fig. 13). All available U-
672 Pb data therefore suggest that the analyzed Chinle Formation strata are Late Triassic, and probably
673 Norian in age (Dickinson, 2018), given the assigned ages of ~ 237 to ~ 201.3 for Late Triassic time (Cohen
674 et al., 2013) and ~ 227 to ~ 208.5 Ma (Cohen et al., 2013) or ~ 205.7 Ma (Kent et al., 2017) for Norian time.

675 Figure 13 presents a comparison of our preferred maximum depositional ages, all available ID- and CA-
676 TIMS ages [from Riggs et al. (2003), Heckert et al. (2009), Ramezani et al. (2011), Irmis et al. (2011),
677 Atchley et al. (2013), Nordt et al., (2015), Kent et al. (2018), and Rasmussen et al. (2020)], and two age
678 models that are based on magnetostratigraphic and CA-TIMS geochronologic information (Kent et al.,
679 2019; Rasmussen et al., 2020). As shown on this figure, our LA-ICPMS MDA's reveal two first-order
680 patterns. The first pattern is that the LA-ICPMS-based MDA's overlap with most CA-TIMS ages and both
681 age models for most strata belonging to the Blue Mesa Member and Petrified Forest Member, but are
682 significantly older for strata of the Sonsela Member. The second pattern is that most LA-ICPMS-based
683 MDA's belong to three main clusters (~ 222 - 219 Ma, ~ 217 - 215 Ma, and ~ 212 - 211 Ma), whereas the other
684 chronologic records show a relatively simple pattern of upward younging (Fig. 13). The following
685 discussion explores these two patterns – details of the magnetostratigraphic information, CA-TIMS data,
686 and age models are discussed by Kent et al. (2018, 2019) and Rasmussen et al. (2020).

687 As shown on Figure 13, the LA-ICPMS-based MDA's presented herein overlap with the other
688 chronometers for sequences which are dominated by fine-grained strata (e.g., Blue Mesa Member and
689 Petrified Forest Member), but are several million years too old for sequences which are dominated by
690 coarse-grained strata (Sonsela Member) (Fig. 13). This pattern appears to hold for member-scale

691 stratigraphic units (e.g., strata from the Petrified Forest Member), although some individual samples
692 clearly do not follow this pattern. For example, of the six samples from the Petrified Forest Member that
693 yield maximum depositional ages which overlap with the other chronometers, four are mudstone-
694 siltstone and two are sandstone. In the lower Sonsela Member, of the six samples that yield maximum
695 depositional ages that predate the other chronometers, five are sandstone and one is siltstone. These
696 exceptions suggest that the dominant lithic characteristics and depositional environment of a member
697 (e.g., dominantly fine-grained floodplain deposits for the Petrified Forest Member versus dominantly
698 coarse-grained channel deposits of the Sonsela Member [Woody, 2006]), are more important than the
699 grain size of an individual horizon in controlling the recognition of near-depositional-age zircon grains.

700 The observed pattern that predominantly fine-grained strata of the Mesa Redondo, Blue Mesa, and
701 Petrified Forest members yield reliable MDA's, whereas predominantly coarse-grained sandstones of
702 the Sonsela Member do not, is surprising for two reasons. First, in terms of provenance (as described
703 above), strata of the Mesa Redondo, Blue Mesa, and Petrified Forest members are interpreted to have
704 been shed mainly from the Ouachita orogen, which lacks Triassic igneous rocks, whereas strata of the
705 Sonsela Member were shed from the Cordilleran magmatic arc to the southwest, which contains
706 abundant Permian and Triassic igneous rocks (Fig. 3). Second, as shown in the margins of Figures 7 and
707 8, Triassic zircon grains are significantly (~2x) more abundant in strata of the Sonsela Member than in
708 underlying and overlying strata. Based on these two observations, one might expect that strata of the
709 Sonsela Member would yield reliable MDA's, whereas strata from the Mesa Redondo Member, Blue
710 Mesa Member, and Petrified Forest Member would not.

711 We suggest that these counter-intuitive relations result in large part from our analytical method of only
712 analyzing zircon grains that are >60 μm , combined with the maximum size of zircons that can be
713 transported in fine-grained versus coarse-grained sediments. For coarse-grained sediment, >60 μm
714 zircon grains could include both transported (detrital) components that predate deposition, as well as
715 zircons that are air-fall in origin and approximately of depositional age. A MDA calculated from a mix of
716 these grains would accordingly pre-date deposition. In contrast, Triassic zircon grains from fine-grained
717 strata would tend to be mostly air-fall in origin given that the older, transported grains are too small to
718 analyze. A MDA calculated from zircons that are primarily of air-fall origin would accordingly approach
719 the true depositional age.

720 The relations described above suggest that convergence versus divergence of the chronologic records
721 results from connections between depositional setting, grain size, provenance, and analytical methods,

722 which together conspire to control the proportions of air-fall (near-depositional age) versus slightly
723 older detrital zircon grains recognized in our samples. We suggest that the three chronometric records
724 agree (to within ~1 m.y.) for strata of the lower Blue Mesa Member and middle-upper Petrified Forest
725 Member because of the availability of zircon grains of air-fall origin, which are near depositional age and
726 both <60 μm and >60 μm in size, versus the scarcity of pre-depositional-age Triassic grains of sufficient
727 size for analysis due to the lack of Triassic rocks in the source region (mainly the Ouachita orogen) and
728 the small (<60 μm) grain size of most sediment. In contrast, for the Sonsela Member, the LA-ICPMS
729 MDA's are interpreted to pre-date the other chronologic records because the sediment was derived
730 from the south, where abundant igneous rocks of Permian-Triassic age were exposed, and the grain size
731 of the detrital (pre-depositional-age) zircons was sufficiently large that many would have been analyzed.

732 A test of this hypothesis is provided by MSWD values of the weighted means calculated for ages from
733 samples belonging to the various stratigraphic units. As shown in DR Table 6, average MSWD values for
734 samples from dominantly fine-grained strata of the Mesa Redondo-Blue Mesa and Petrified Forest units
735 are 1.7 and 1.3 (respectively), whereas coarser grained strata of the lower and upper Sonsela units yield
736 higher MSWD values of 2.6 and 2.1 (respectively). These values are consistent with the interpretation
737 that Triassic zircon grains in coarser-grained units have a greater range of ages than Triassic zircon grains
738 in finer-grained units.

739 These interpreted connections may also provide an explanation for the patterns of offset of the CA-TIMS
740 ages of Rasmussen et al. (2020) relative to the LA-ICPMS ages and magnetostratigraphic age models in
741 the Sonsela Member (Fig. 13). For strata of the upper Sonsela Member, the CA-TIMS and
742 magnetostratigraphic records converge because the methods of grain selection were apparently
743 successful in identifying populations of syn-depositional age zircon grains. For strata of the lower
744 Sonsela Member, however, these methods were unsuccessful in identifying a sufficient number of
745 depositional-age zircon grains to determine a reliable MDA, presumably because of their low abundance
746 relative to older transported grains.

747 The second main pattern exhibited by the three chronometers is that most of the LA-ICPMS-based
748 MDA's belong to three main clusters (~222-219 Ma, ~217-215 Ma, and ~212-211 Ma), whereas the other
749 chronologic records show a relatively simple pattern of upward younging (Fig. 13). For the ~222-219 Ma
750 cluster, a plausible interpretation, following from the connections described above, is that ~222-219 Ma
751 zircon grains of air-fall origin accumulated in fine-grained strata of the lower Blue Mesa Member, and
752 were then recycled from age-equivalent strata into predominantly coarser grained channel sands of the

753 upper Blue Mesa Member and lower Sonsela Member. Grains from these same sources appear to have
754 also been recycled into sandstone sample 131-2 of the lower Petrified Forest Member (Fig. 13). The
755 ~212-211 Ma cluster may have formed in a similar fashion, with initial accumulation of near-
756 depositional-age air-fall zircons in mudstones of sample 116-1, followed by recycling of these grains
757 from age-equivalent strata into coarser-grained strata of samples 104-3, 92-2, and 84-2 (Fig. 13).

758 The source of zircon grains that belong to the ~217-215 Ma cluster is less obvious given the lack of
759 recognized fine-grained strata dominated by zircons of this age (Fig. 13). One possibility is that ~217-215
760 Ma grains were eroded from fine-grained strata exposed elsewhere [perhaps near Sonsela Buttes
761 (Marsh et al., 2019) or near the Cordilleran magmatic arc] that are dominated by grains of this age. A
762 second possibility is that fine-grained strata dominated by ~217-215 Ma ages were originally present in
763 the lower Sonsela Member, but were removed by erosion and recycled into strata of the upper Sonsela
764 Member. Previous workers have suggested the existence of a hiatus or hiatuses (Ramezani et al., 2011)
765 or an erosional event (Rasmussen et al., 2020) at approximately this stratigraphic level, as shown by the
766 preferred age model of Rasmussen et al. (2020) on Figure 13. The occurrence of very different <240 Ma
767 ages, >240 Ma ages, and U/Th values in samples 196-3 and 195-2 suggests that this shift in provenance,
768 accumulation of a condensed section, or formation of an unconformity likely coincides with the
769 proposed boundary between strata of the lower Sonsela Member and upper Sonsela Member. As
770 discussed by Ramezani et al. (2011) and Rasmussen et al. (2020), the possibility of an unconformity or
771 condensed section near this stratigraphic position has important implications for Chinle stratigraphy and
772 fundamental Late Triassic biotic and climatic changes. It should be noted, however, that no stratigraphic
773 evidence for such an unconformity was recognized in the CPCP core.

774 **10. IMPLICATIONS FOR THE STRATIGRAPHY OF THE CHINLE FORMATION**

775 The interpreted connections between the three geochronologic records and Chinle stratigraphy
776 provide an opportunity to reconstruct the depositional history of the Chinle Formation.
777 Fundamental assumptions in reconstructing this history are that:

778 (1) Chinle Formation strata encountered in the CPCP core record nearly continuous deposition
779 as described in the age model of Kent et al. (2019), perhaps with a period of erosion or very
780 slow deposition in the middle part of the Sonsela Member (Rasmussen et al., 2020).

781 (2) LA-ICPMS ages recovered from strata of the Chinle Formation belong to five separate groups
782 (red vertical bars of Figure 13) due to the hypothesized connections between stratigraphy, grain
783 size, and proportions of near-depositional-age (air-fall) versus older (recycled) zircon ages.

784 (3) Late Triassic igneous activity in the Cordilleran magmatic arc provided a nearly continuous
785 supply of zircon grains of air-fall origin to the Chinle deposystem. This assumption is supported
786 by the relatively continuous distribution of U-Pb ages within the Cordilleran magmatic arc and
787 back-arc (upper curves of Figure 13). This view is in contrast to the hypothesis of Kent et al.
788 (2019) that variations in the proportions of depositional-age versus older zircon grains result
789 mainly from temporal changes in magmatic flux.

790 The interpreted stratigraphic evolution is summarized below and shown schematically on
791 Figure 14. Important phases in this evolution are as follows:

792 A: An LA-ICPMS MDA of ~ 223.3 Ma from our one sample from the Mesa Redondo Member
793 (305-2) agrees with the magnetostratigraphic information, the two age models, and the set of
794 CA-TIMS ages from this sample, presumably because these fine-grained strata are dominated
795 by zircon grains of air-fall origin. Older CA-TIMS ages of ~ 225.2 Ma (Ramezani et al., 2011) and
796 ~ 227.6 (Atchley et al., 2013) from outcrops of the Mesa Redondo Member may be
797 compromised by an abundance of recycled zircon grains.

798 B: LA-ICPMS ages of ~ 221 Ma from fine-grained strata in the lower part of the Blue Mesa
799 Member are also near depositional age, presumably because the >60 μm zircon grains in these
800 fine-grained strata are dominated by air-fall (or slightly reworked) components.

801 C: LA-ICPMS ages from strata of the upper Blue Mesa Member significantly pre-date deposition,
802 presumably because these strata are dominated by recycled zircons. The predominance of ~ 221
803 Ma LA-ICPMS MDA's suggests that most zircon grains were recycled from lateral equivalents of
804 underlying strata in the lower part of the Blue Mesa Member. CA-TIMS ages also pre-date
805 deposition, presumably because of the difficulty of isolating near-depositional-age grains of air-
806 fall origin.

807 D: This pattern continues up through most of the lower Sonsela Member, with LA-ICPMS MDA's
808 remaining at ~ 221 due to recycling of strata from lateral equivalents of the lower Blue Mesa
809 Member. Most CA-TIMS ages predate the age of deposition because depositional-age (air fall)
810 grains were diluted by recycled components.

811 E: The age patterns from sandstones of the upper Sonsela Member are somewhat puzzling
812 given that the dominant ~ 217 - 215 Ma LA-ICPMS MDA's pre-date deposition, but fine-grained
813 strata that could have sourced grains of these ages are not present in the lower Sonsela
814 Member (Fig. 13). One possibility, as described above, is that the ~ 217 - 215 Ma grains were
815 eroded from fine-grained strata exposed elsewhere [perhaps near Sonsela Buttes (Marsh et al.,
816 2019) or from the Cordilleran magmatic arc] that are dominated by grains of this age. A second
817 possibility is that fine-grained strata dominated by ~ 217 - 215 Ma ages were originally present in
818 the underlying lower Sonsela Member, but were removed by erosion and recycled into strata of
819 the upper Sonsela Member. An erosional event of the appropriate age and stratigraphic
820 position has been described by Ramezani et al. (2011) and by Rasmussen et al. (2020), as shown
821 by their age model on Figure 13. The occurrence of very different <240 Ma ages, >240 Ma ages,

822 and U/Th values in samples 196-3 and 195-2 suggests that this change in provenance,
823 condensed section, or unconformity most likely coincides with the boundary between lower
824 and upper Sonsela Member strata. As discussed by Rasmussen et al. (2020), the possibility of an
825 unconformity or condensed section near this stratigraphic position has important implications
826 for Chinle stratigraphy and fundamental Late Triassic biotic and climatic changes.

827 F: The dominance of pre-depositional-age grains in sample 131-2 provides strong evidence for
828 recycling of detrital zircons from lateral equivalents of underlying strata of the Blue Mesa
829 Member or lower Sonsela Member.

830 G: All chronometers agree for strata of sample 116-1, presumably because these fine-grained
831 strata are dominated by air-fall (or slightly reworked) detrital zircons.

832 H: LA-ICPMS MDA's from sandstones of the middle Petrified Forest Member (samples 104-3,
833 92-2, and 84-2) slightly predate deposition because they were recycled from lateral equivalents
834 of immediately underlying fine-grained strata (e.g., sample 116-1).

835 I: All chronometers agree for strata of the Black Forest bed because this unit is dominated by
836 air-fall (or slightly reworked) detrital zircon grains.

837 **11. CONCLUSIONS**

838 First-order conclusions that result from our U-Pb geochronologic analyses of detrital zircon
839 grains from the Coconino Sandstone, Moenkopi Formation, and Chinle Formation are as
840 follows:

841 1. The provenance of strata belonging to the Coconino Sandstone and Moenkopi Formation can
842 be reconstructed by comparison of our LA-ICPMS ages (Figures 5 and 6) with age distributions
843 that characterize potential source regions (Figure 3). As shown on Figures 5 and 11, data from
844 our sample of the Coconino Sandstone and equivalent sandstones of the southern Colorado
845 Plateau suggest that these strata belong to an eolian blanket that was derived largely from the
846 Ouachita and/or Appalachian orogens, whereas strata from the northern Colorado Plateau
847 consist mainly of sediment derived from local basement uplifts (Fig. 1; Dickinson and Gehrels,
848 2003; Gehrels et al., 2011; Lawton et al. (2015). Lower-Middle Triassic strata of the Moenkopi
849 Formation record a very different dispersal system, with most detritus derived from the
850 Ouachita orogen, the East Mexico arc, and early phases of the Cordilleran magmatic arc (Figures
851 6 and 9).

852 2. LA-ICPMS ages from strata of the Chinle Formation belong to five groups that generally
853 correspond to the main stratigraphic units (Figures 7, 8, and 13). Maximum depositional ages
854 calculated from <240 Ma ages and provenance interpretations derived from >240 Ma ages are
855 as follows:

856 -- Strata of the Mesa Redondo Member yield a preferred MDA of ~223.3 Ma, and were derived
857 mainly from the Ouachita orogen.

858 -- Strata of the Blue Mesa Member yield MDA's of ~220.7 to ~220.2 Ma, and were derived from
859 local basement and Ouachita sources.

860 -- Strata in the lower part of the Sonsela Member yield similar MDA's of ~220.9 to ~220.3 Ma
861 (plus an uppermost sample with an MDA of ~218.2 Ma). Detritus was derived mainly from local
862 basement (especially ~1.44 Ga) sources, perhaps located in the ancestral Mogollon highlands to
863 the south.

864 -- Strata in the upper part of the Sonsela Member yield younger MDA's of ~216.6 to ~215.1 Ma,
865 plus an uppermost sample with an MDA of ~213.8 Ma. Grains with >240 Ma ages were derived
866 mainly from Precambrian basement (mainly ~1.44 Ga) and Grenville-age rocks to south, as well
867 as the East Mexico arc.

868 -- Strata of the Petrified Forest Member yield ages that belong to three separate groups. The
869 lowest sample yields an MDA of ~221.5, which is significantly older than ages from adjacent
870 strata. The middle four samples yield MDA's of ~211.7 to ~211.2 Ma, whereas the upper two
871 samples yield MDA's of ~209.8 and ~209.6 Ma. All six upper samples contain abundant >240 Ma
872 grains that were shed from a broad range of Ouachita, local basement, and East Mexico arc
873 sources.

874 3. Patterns of U and Th concentration in Triassic zircon grains from the Chinle Formation belong
875 to four distinct groups that generally coincide with the chronostratigraphic units described
876 above. Changes in U and Th concentrations are interpreted to record variations in the chemistry
877 of arc magmatism through time, as has been documented previously by Barth and Wooden
878 (2006, 2011, 2013) and Riggs et al. (2010, 2012, 2016).

879 4. Comparison of the Chinle Formation MDA's with magnetostratigraphic information (Kent et
880 al., 2018, 2019) and CA-TIMS geochronologic information (Rasmussen et al., 2020) from the
881 CPCP core, plus CA-TIMS ages reported from outcrop samples, indicates that LA-ICPMS MDA's
882 approximate depositional ages for most strata of the Mesa Redondo Member, Blue Mesa
883 Member, and Petrified Forest Member, but significantly pre-date deposition for strata of the
884 Sonsela Member (Fig. 13). The correlation of age patterns with stratigraphy is interpreted to
885 reflect the proportions of air-fall (or slightly reworked) versus recycled (older) zircon grains:
886 fine-grained strata are dominated by near-depositional ages because most zircon grains are air-
887 fall (or slightly reworked) in origin, whereas coarse-grained strata are dominated by pre-
888 depositional ages because recycled zircon grains dilute the abundance of air-fall crystals.

889 5. This hypothesized connection between stratigraphy and the three geochronologic records
890 supports the following depositional history for Chinle Formation strata encountered in the CPCP
891 core (Figures 13 and 14):

892 -- LA-ICPMS ages and magnetostratigraphic information (Kent et al., 2019) indicate that the
893 sampled part of the Mesa Redondo Formation was deposited at ~223.3 Ma. CA-TIMS ages of
894 ~225.2 Ma (Ramezani et al., 2011) and ~227.6 (Atchley et al., 2013) from outcrop samples

895 suggest that strata of the Mesa Redondo Member in other areas are dominated by older
896 recycled components.

897 -- Magnetostratigraphic information (Kent et al., 2019) suggests that strata of the Blue Mesa
898 Member and lower Sonsela Member accumulated between ~222 Ma and ~214 Ma, whereas
899 LA-ICPMS MDA's are consistently ~221 Ma for the same strata (except for the uppermost
900 sample of ~217 Ma). This suggests that most zircons in strata of the upper Blue Mesa Member
901 and lower Sonsela Member were recycled from lateral equivalents of strata of the lower Blue
902 Mesa Member. The observation that most CA-TIMS ages from these strata also pre-date
903 deposition is interpreted to result from the dilution of air-fall zircon crystals by older recycled
904 zircon grains.

905 -- Strata of the upper Sonsela Member accumulated between ~215 and ~213 Ma, as
906 constrained by magnetostratigraphic information and CA-TIMS ages. LA-ICPMS MDAs from
907 these strata are ~217-215 Ma, which indicates that they are dominated by zircons recycled
908 from older units. The lack of samples in the lower Sonsela Member that are dominated by
909 ~217-215 Ma grains suggests that zircon grains of this age in upper Sonsela Member strata may
910 have been transported from sections of the Chinle Formation exposed outside of the PEFO
911 area. It is also possible that such strata were exposed in the PEFO area, but were removed
912 during an erosional event inferred by Rasmussen et al. (2020) from the pattern of CA-TIMS ages
913 in the upper Sonsela Member (Fig. 3). Significant changes in <240 Ma ages, >240 Ma ages, and
914 U-Th values suggest that this unconformity, if present, occurs between samples 196-3 and 195-
915 2.

916 -- All available evidence suggests that mudstone and subordinate sandstone of the middle
917 Petrified Forest Member accumulated at ~212-211 Ma, and the Black Forest bed in the upper
918 part of the unit accumulated at ~210 Ma. In contrast, LA-ICPMS ages recovered from sample
919 131-2, from the lower part of the Petrified Forest Member, are dominantly ~221 Ma, suggestive
920 of recycling from lateral equivalents of strata of the Blue Mesa Member and lower Sonsela
921 Member.

922 6. Comparisons of our LA-ICPMS ages, the available CA-TIMS data, and magnetostratigraphic
923 information provide insights into methods for determining the depositional age of fluvial strata.
924 Our results show that the most reliable information comes from sequences dominated by fine-grained
925 clastic strata (mudstone and siltstone) given that these strata have a low abundance of pre-depositional-
926 age zircon grains of the appropriate size (>60 μm diameter) for routine analysis by LA-ICPMS. Mudstone-
927 siltstone samples may accordingly yield a high proportion of >60 μm zircon grains that are air-fall in
928 origin (or only slightly reworked) and thereby record the age of deposition. In contrast, sedimentary
929 sequences dominated by sandstone could well yield abundant >60 μm zircon grains that predate
930 deposition, thereby diluting syn-depositional-age zircon grains. Future attempts to determine
931 depositional ages from fluvial strata should accordingly focus on sequences dominated by fine-grained
932 strata, rather than sandstones, in spite of the challenges of extracting and analyzing the smaller zircon
933 crystals.

934 **12. AUTHOR CONTRIBUTION**

935 NG and GG generated the LA-ICPMS data reported in this paper. All coauthors were involved in
936 acquiring the samples that were analyzed and/or interpreting the data. GG prepared this
937 manuscript with input from all co-authors.

938 **13. COMPETING INTERESTS**

939 The authors declare that they have no conflict of interest.

940 **14. ACKNOWLEDGEMENTS**

941 Geochronologic analyses were conducted with support from NSF EAR-0959107 and EAR-
942 1649254 (to Gehrels). Laboratory analyses were performed primarily by N. Giesler.
943 Collaborative aspects of the project were supported by NSF EAR 0958976 (PEO & JWG),
944 0958723 (RM), 0958915 (RBI), and 0958859 (DVK). Funding for coring and much logistical
945 support was provided by ICDP (International Scientific Continental Drilling Program grant 05-
946 2010: JWG, PEO, Jingeng Sha, Roberto Molina-Garza, Wolfram Kürschner, and Gerhard
947 Bachmann). Additional funding was supplied by grants from the Lamont Climate Center (PEO).
948 Field support was provided by LacCore personnel (Anders Noren, Kristina Brady, and Ryan
949 O'Grady), drilling manager Doug Schnurrenberger, and core-handling volunteers (Justin Clifton,
950 Bob Graves, Ed Lamb, Max Schnurrenberger, and Riley Black). Superintendent Brad Traver of
951 the National Park Service arranged for permission to core in the PEFO and provided logistical
952 support during site selection and drilling. This is Petrified Forest Paleontological Contribution 67.
953 The conclusions presented here are those of the authors and do not represent the views of the
954 United States Government.

955 **REFERENCES CITED**

- 956 Alsalem, O.B., Fan, M., Zamora, J., Xie, X., and Griffin, W.R.: Paleozoic sediment dispersal before
957 and during the collision between Laurentia and Gondwana in the Fort Worth Basin, USA:
958 *Geosphere*, v. 14, no. 1, p. 1–18, doi: 10.1130/GES01480.1, 2018.
- 959 Ash, S.R.: The Black Forest Bed, a distinctive unit in the Upper Triassic Chinle Formation, north-
960 eastern Arizona: *Journal of the Arizona-Nevada Academy of Science*, v. 24–25, p. 59–73, 1992.
- 961 Atchley, S.C., Nordt, L.C., Dworkin, S.I., Ramezani, J., Parker, W.G., Ash, S.R., and Bowring, S.A.:
962 A linkage among Pangean tectonism, cyclic alluviation, climate change, and biologic turnover in
963 the Late Triassic: The Record from the Chinle Formation, Southwestern United States: *Journal of*
964 *Sedimentary Research*, v. 83, p. 1147–1161, 2013.
- 965 Baranyi, V., Reichgelt, T., Olsen, P.E., Parker, W.G., Kürschner, W.M.: Norian vegetation history
966 and related environmental changes: new data from the Chinle Formation, Petrified Forest
967 National Park (Arizona, SW USA): *Geological Society of America Bulletin*, v. 130, p. 775–795,
968 doi.org/10.1130/B31673.1, 2017.
- 969 Barth, A.P. and Wooden, J.L.: Timing of magmatism following initial convergence at a passive
970 margin, southwestern US Cordillera, and ages of lower crustal magma sources: *Journal of*
971 *Geology*, v. 114, p. 231–245, 2006.
- 972 Barth, A.P., Walker, J.D., Wooden, J.L., Riggs, N.R., and Schweickert, R.A.: Birth of the Sierra
973 Nevada magmatic arc: Early Mesozoic plutonism and volcanism in the east-central Sierra
974 Nevada of California: *Geosphere*, v. 7, p. 877–897, 2011.
- 975 Barth, A.P., Wooden, J.L., Jacobson, C.E., and Economos, R.C.: Detrital zircon as a proxy for
976 tracking the magmatic arc system: The California arc example: *Geology*, v. 41, p. 223–226, 2013.
- 977 Black, L., Kamo, S., Allen, C., Davis, D., Aleinikoff, J., Valley, J., Mundil, R., Campbell, I., Korsch,
978 R., Williams, I., and Foudoulis, C.: Improved $^{206}\text{Pb}/^{238}\text{U}$ microprobe geochronology by the
979 monitoring of a trace-element-related matrix effect; SHRIMP, ID-TIMS, ELA-ICP-MS and
980 oxygen isotope documentation for a series of zircon standards: *Chemical Geology*, v. 205, p.
981 115–140, 2004.
- 982 Blakey, R.C., Peterson, F., and Kocurek, G.: Synthesis of late Paleozoic and Mesozoic eolian
983 deposits of the western interior of the United States: *Sedimentary Geology*, v. 56, p. 3–125,
984 1988.
- 985 Chen, J.H., and Moore, J.G.: Uranium-lead isotopic ages from the Sierra Nevada batholith:
986 *Journal of Geophysical Research*, v. 87, p. 4761–4784, 1982.
- 987 Cohen, K.M., Finney, S.C., Gibbard, P.L., and Fan, J.-X.: The ICS International Chronostratigraphic
988 Chart: Episodes v. 36, p. 199–204 (updated 2018), 2013.

- 989 Creber, G.T., and Ash, S.R.: Evidence of widespread fungal attack on Upper Triassic trees in the
990 southwestern U.S.A.: *Review of Palaeobotany and Palynology*, v. 63, p. 189-195, 1990.
- 991 DeGraaff-Surples, K., Graham, S.A., Wooden, J.L., and McWilliams, M.O.: Detrital zircon
992 provenance analysis of the Great Valley Group, California: Evolution of an arc-forearc system:
993 *Geological Society of America Bulletin*, v. 114 (12), p. 1564–1580, 2002.
- 994 Dickinson, W.R.: Tectonosedimentary Relations of Pennsylvanian to Jurassic strata on the
995 Colorado Plateau, *Geological Society of America Special Paper 533*, 184 p., 2018.
- 996 Dickinson, W.R., and Gehrels, G.E.: U-Pb ages of detrital zircon grains from Permian and Jurassic
997 eolian sandstones of the Colorado Plateau, USA: Paleogeographic implications: *Sedimentary
998 Geology*, v. 163, p. 29–66, 2003.
- 999 Dickinson, W.R. and Gehrels, G.E.: U-Pb ages of detrital zircon grains in relation to
1000 paleogeography: Triassic paleodrainage networks and sediment dispersal across southwest
1001 Laurentia: *Journal of Sedimentary Research*, v. 78, p. 745–764, 2008.
- 1002 Dickinson, W.R. and Gehrels, G.E.: Use of U–Pb ages of detrital zircon grains to infer maximum
1003 depositional ages of strata: a test against a Colorado Plateau Mesozoic database: *Earth and
1004 Planetary Science Letters*, v. 288, p. 115–125, 2009.
- 1005 Gehrels, G.E.: Introduction to detrital zircon studies of Paleozoic and Triassic strata in western
1006 Nevada and northern California, in Soreghan, M.J. and Gehrels, G.E., eds., *Paleozoic and Triassic
1007 paleogeography and tectonics of western Nevada and northern California: Geological Society of
1008 America Special Paper 347*, p. 1-18, 2000.
- 1009 Gehrels, G.E.: Detrital zircon U-Pb geochronology applied to tectonics: *Annual Review of Earth
1010 and Planetary Sciences*, v. 42, p. 127-149, 2014.
- 1011 Gehrels, G. and Pecha, M.: Detrital zircon U-Pb geochronology and Hf isotope geochemistry of
1012 Paleozoic and Triassic passive margin strata of western North America: *Geosphere*, v. 10 (1), p.
1013 49-65, 2014.
- 1014 Gehrels, G.E., Valencia, V., Pullen, A.: Detrital zircon geochronology by Laser-Ablation
1015 Multicollector ICPMS at the Arizona LaserChron Center, in Loszewski, T., and Huff, W., eds.,
1016 *Geochronology: Emerging Opportunities*, *Paleontology Society Short Course: Paleontology
1017 Society Papers*, v. 11, 10 p., 2006.
- 1018 Gehrels, G.E., Valencia, V., Ruiz, J.: Enhanced precision, accuracy, efficiency, and spatial
1019 resolution of U-Pb ages by laser ablation–multicollector–inductively coupled plasma–mass
1020 spectrometry: *Geochemistry, Geophysics, Geosystems*, v. 9, Q03017,
1021 doi:10.1029/2007GC001805, 2008.

- 1022 Gehrels, G., Blakey, R., Karlstrom, K., Timmons, M., Dickinson, W., and Pecha, M.: Detrital zircon
1023 U-Pb geochronology of Paleozoic strata in the Grand Canyon: *Lithosphere*, v. 3 (3), p. 183-200,
1024 2011.
- 1025 González-León, C.M., Valencia, V.A., Lawton, T.F., Amato, J.M., Gehrels, G.E., Leggett, W.J.,
1026 Montijo-Contreras, O., Fernández, M.A.: The lower Mesozoic record of detrital zircon U-Pb
1027 geochronology of Sonora, México, and its paleogeographic implications: *Revista Mexicana de*
1028 *Ciencias Geológicas*, v. 26 (2), p. 301-314, 2009.
- 1029 Heckert, A.B. and Lucas, S.G.: Revised Upper Triassic stratigraphy of the Petrified Forest
1030 National Park, Arizona, USA: *New Mexico Museum of Natural History Science Bulletin*, v. 21, p.
1031 1–36, 2002.
- 1032 Heckert, A.B., Lucas, S.G., Dickinson, W.R., and Mortensen, J.K.: New ID-TIMS U-Pb ages for
1033 Chinle Group strata (Upper Triassic) in New Mexico and Arizona, correlation to the Newark
1034 Supergroup, and implications for the “long Norian”: *Geological Society of America Abstracts*
1035 *with Programs*, v. 41, p. 123, 2009.
- 1036 Hildebrand, R.S.: Did westward subduction cause Cretaceous-Tertiary orogeny in the North
1037 American Cordillera?: *Geological Society of America Special paper* 457, 71 p., 2009.
- 1038 Hildebrand, R.S.: Mesozoic assembly of the North American cordillera: *Geological Society of*
1039 *America Special paper* 495, 169 p., 2013.
- 1040 Hoke, G., Schmitz, M., and Bowring, S.: An ultrasonic method for isolating nonclay components
1041 from clay-rich material: *Geochemistry Geophysics Geosystems*, v. 15, p. 492–498, 2014.
- 1042 Horstwood, M., Kosler, J., Gehrels, G., Jackson, S., McLean, N., Paton, C., Pearson, N., Sircombe,
1043 K., Sylvester, P., Vermeesch, P., Bowring, J., Condon, D., and Schoene, B.: Community-Derived
1044 Standards for LA-ICP-MS U-Th-Pb Geochronology – Uncertainty Propagation, Age Interpretation
1045 and Data Reporting: *Geostandards and Geoanalytical Research*, v. 40 (3), p. 311-332, 2016.
- 1046 Irmis, R.B., Mundil, R., Martz, J.W., and Parker, W.G.: High-resolution U-Pb ages from the Upper
1047 Triassic Chinle Formation (New Mexico, USA) support a diachronous rise of dinosaurs: *Earth and*
1048 *Planetary Science Letters*, v. 309, p. 258–267, 2011.
- 1049 Kent, D.V., Olsen, P.E., and Muttoni, G.: Astrochronostratigraphic polarity time scale (APTS) for
1050 the Late Triassic and Early Jurassic from continental sediments and correlation with standard
1051 marine stages: *Earth-Science Reviews*, v. 166, p. 153–180, 2017.
- 1052 Kent, D.V., Olsen, P.E., Rasmussen, C., Lepre, C.J., Mundil, R., Irmis, R.B., Gehrels, G.E., Giesler,
1053 D., Geissman, J.W., and Parker, W.G.: Empirical evidence for stability of the 405 kyr Jupiter-
1054 Venus eccentricity cycle over hundreds of millions of years: *Proceedings of the National*
1055 *Academy of Sciences*, v. 115, p. 6153–6158, 2018.

1056 Kent, D.V., Olsen, P.E., Lepre, C. Mundil, R., Rasmussen, C., Irmis, R.B., Gehrels, G.E., Giesler, D.,
1057 Geissman, J.W., Parker, W.G.: Magnetostratigraphy of the entire Chinle Formation (Norian age)
1058 in scientific drill core PFNP-1A from the Petrified Forest National Park (Arizona, USA) and
1059 implications for global correlations in the Late Triassic: *Geophysics, Geochemistry, Geosystems*
1060 (in review), 2019.

1061 Kiscock, J.K., Finzel, E.S., Malone, D.H., and Craddock, J.P.: Lower–Middle Pennsylvanian strata
1062 in the North American midcontinent record the interplay between erosional unroofing of the
1063 Appalachians and eustatic sea-level rise: *Geosphere*, v. 14 (1), p. 141–161, 2018.

1064 Lawton, T.F., Buller, C.D., and Parr, T.R.: Provenance of a Permian erg on the western margin of
1065 Pangea: Depositional system of the Kungurian (late Leonardian) Castle Valley and White Rim
1066 sandstones and subjacent Cutler Group, Paradox Basin, Utah, USA: *Geosphere*, v. 11 (5), p. 1–
1067 32, 2015.

1068 Lucas, S.G.: The Chinle Group: revised stratigraphy and biostratigraphy of Upper Triassic
1069 nonmarine strata in the western United States, in: *Aspects of Mesozoic Geology and*
1070 *Paleontology of the Colorado Plateau*, edited by: Morales, M., Museum of Northern Arizona
1071 Bulletin 59, Flagstaff: Museum of Northern Arizona Press, p. 27–50., 1993.

1072 Ludwig, K.R.: Isoplot 3.6: Berkeley Geochronology Center Special Publication 4, 77 p., 2008.

1073 Marsh, A.D., Parker, W.G., Stockli, D.F., and Martz, J.W.: Regional correlation of the Sonsela
1074 Member (Upper Triassic Chinle Formation) and detrital U-Pb zircon data from the Sonsela
1075 Sandstone bed near the Sonsela Buttes, northeastern Arizona, USA, support the presence of a
1076 distributive fluvial system: *Geosphere*, v. 15, <https://doi.org/10.1130/GES02004.1>, 2019.

1077 Martz, J.W. and Parker, W.G.: Revised lithostratigraphy of the Sonsela Member (Chinle
1078 Formation, Upper Triassic) in the southwestern part of Petrified Forest National Park, Arizona:
1079 PLoS ONE 5(2): e9329. doi:10.1371/journal.pone.0009329, 2010.

1080 Martz, J.W., Parker, W.G., Skinner, L., Raucchi, J.J., Umhoefer, P., and Blakey, R.C.: Geologic map
1081 of Petrified Forest National Park, Arizona: Arizona Geological Survey Contributed Map CM-12-A,
1082 1 map sheet, scale 1:50,000, 18 p., http://repository.azgs.gov/uri_gin/azgs/dlio/1487, 2012.

1083 Martz, J.W., Kirkland, J.I., Milner, A.R.C., Parker, W.G., Santucci, V.L.: Upper Triassic
1084 lithostratigraphy, depositional systems, and vertebrate paleontology across southern Utah:
1085 *Geology of the Intermountain West*, v. 4, p. 99-180, [https://www.utahgeology.org/wp-](https://www.utahgeology.org/wp-content/uploads/2018/05/GIW2017-v04-pp099-180-Martz.pdf)
1086 [content/uploads/2018/05/GIW2017-v04-pp099-180-Martz.pdf](https://www.utahgeology.org/wp-content/uploads/2018/05/GIW2017-v04-pp099-180-Martz.pdf), 2017.

1087 Miller, J.S., Glazner, A.F., Walker, J.D., and Martin, M.W.: Geochronologic and isotopic evidence
1088 for Triassic–Jurassic emplacement of the eugeoclinal allochthon in the Mojave Desert region,
1089 California: *Geological Society of America Bulletin*, v. 107, p. 1441–1457, 1995.

- 1090 Nordt, L., Atchley, S., Dworkin, S.: Collapse of the Late Triassic megamonsoon in western
1091 equatorial Pangea, present-day American southwest: *Geological Society of America Bulletin*, v.
1092 127 (11/12), p. 1798–1815, 2015.
- 1093 Olsen, P. E., Kent, D.V., and Whiteside, H.: Implications of the Newark Supergroup-based
1094 astrochronology and geomagnetic polarity time scale (Newark-APTS) for the tempo and mode
1095 of the early diversification of the Dinosauria: *Earth and Environmental Science Transactions of*
1096 *the Royal Society of Edinburgh*, v. 101, p. 201–229, 2011.
- 1097 Olsen, P., Geissman, J., Kent, D., Gehrels, G., and 23 others: Colorado Plateau Coring Project,
1098 Phase I (CPCP-I): a continuously cored, globally exportable chronology of Triassic continental
1099 environmental change from western North America: *Scientific Drilling*, v. 24, p. 15–40, 2018.
- 1100 Olsen, P.E., Laskar, J., Kent, D.V., Kinney, S.T., Reynolds, D.J., Sha, J. and Whiteside, J.H.:
1101 Mapping Solar System chaos with the Geological Orrery: *Proceedings of the National Academy*
1102 *of Sciences*, v. 116 (22), p. 10664-10673, 2019.
- 1103 Ortega-Flores, B., Solari, L., Lawton, T.F., and Ortega-Obregón, C.: Detrital-zircon record of
1104 major Middle Triassic–Early Cretaceous provenance shift, central Mexico: demise of
1105 Gondwanan continental fluvial systems and onset of backarc volcanism and sedimentation:
1106 *International Geology Review*, v. 56 (2), p. 237-261, 2014.
- 1107 Paces, J.B., & Miller, J.D.: Precise U-Pb ages of Duluth Complex and related mafic intrusions,
1108 northeastern Minnesota: Geochronological insights to physical, petrogenetic, paleomagnetic,
1109 and tectonomagmatic processes associated with the 1.1 Ga midcontinent rift system: *Journal of*
1110 *Geophysical Research*, v. 98 (B8), p. 13997–14013. <https://doi.org/10.1029/93JB01159>, 1993.
- 1111 Parker, W., and Martz, J.: Constraining the stratigraphic position of the Late Triassic (Norian)
1112 Adamanian-Revueltian faunal transition in the Chinle Formation of Petrified Forest National
1113 Park, Arizona: *Journal of Vertebrate Paleontology*, v. 29 (suppl. to 3), p. 162A, 2009.
- 1114 Parker, W.G., and Martz, J.W.: The Late Triassic (Norian) Adamanian–Revueltian tetrapod faunal
1115 transition in the Chinle Formation of Petrified Forest National Park, Arizona, *Earth and*
1116 *Environmental Science Transactions of the Royal Society of Edinburgh*: v. 101, p. 231–260,
1117 2011.
- 1118 Pipiringos, G.N., O’Sullivan, R.B.: Principal unconformities in Triassic and Jurassic rocks, Western
1119 Interior United States – a preliminary survey: *Geological Survey Professional Paper 1035-A*, 29
1120 p., 1978.
- 1121 Pullen, A., Ibanez-Mejia, M., Gehrels, G., Giesler, D., and Pecha, M.: Optimization of a Laser
1122 Ablation-Single Collector-Inductively Coupled Plasma-Mass Spectrometer (Thermo Element 2)
1123 for Accurate, Precise, and Efficient Zircon U-Th-Pb Geochronology: *Geochemistry, Geophysics,*
1124 *Geosystems*, v. 19. <https://doi.org/10.1029/2018GC007889>, 2018.

- 1125 Ramezani, J., Hoke, G.D., Fastovsky, D.E., Bowring, S.A., Therrien, F., Dworkin, S.I., Atchley, S.C.,
1126 and Nordt, L.C.: High precision U-Pb zircon geochronology of the Late Triassic Chinle Formation,
1127 Petrified Forest National Park (Arizona, USA): Temporal constraints on the early evolution of
1128 dinosaurs: *Geological Society of America Bulletin*, v. 123, p. 2142–2159, 2011.
- 1129 Ramezani, J., Fastovsky, D.E., and Bowring, S.A.: Revised chronostratigraphy of the lower Chinle
1130 Formation strata in Arizona Arizona and New Mexico (USA): high-precision U-Pb
1131 geochronological constraints on the Late Triassic evolution of dinosaurs: *American Journal of
1132 Science*, v. 314, p. 981–1008, 2014.
- 1133 Rasmussen, C., Mundil, R., Irmis, R.B., Geisler, D., Gehrels, G.E., Olsen, P.E., Kent, D.V., Lepre, C.,
1134 Geissmann, J.W., and Parker, W.G.: A high-resolution age model for the Upper Triassic Chinle
1135 Formation (Petrified Forest National Park, Arizona, USA) constrained by U-Pb geochronology
1136 and magnetostratigraphy: implications for Late Triassic paleoecological and
1137 paleoenvironmental change: *Geological Society of America Bulletin* (in review), 2020.
- 1138 Reichgelt, T., Parker, W.G., Martz, J.W., Conran, J.G., Cittert, J.H.A.K., Kürschner, W.M.: The
1139 palynology of the Sonsela Member (Late Triassic, Norian) at Petrified Forest National Park,
1140 Arizona, USA: *Review of Palaeobotany and Palynology*, v. 189, p. 18–28,
1141 doi.org/10.1016/j.revpalbo.2012.11.001, 2013.
- 1142 Riggs, N.R., Lehman, T.M., Gehrels, G.E., and Dickinson, W.R.: Detrital zircon link between
1143 headwaters and terminus of the Upper Triassic Chinle–Dockum paleoriver system: *Science*, v.
1144 273, p. 97–100, 1996.
- 1145 Riggs, N.R., Ash, S.R., Barth, A.P., Gehrels, G.E., and Wooden, J.L.: Isotopic age of the Black
1146 Forest Bed, Petrified Forest Member, Chinle Formation, Arizona: an example of dating a
1147 continental sandstone: *Geological Society of America Bulletin*, v. 115, p. 1315–1323, 2003.
- 1148 Riggs, N.R., Barth, A.P., González-León, C., Jacobson, C.E., Howell, E., Wooden, J.E., and Walker,
1149 J.D.: Provenance of Upper Triassic strata in southwestern North America as suggested by
1150 isotopic analysis and chemistry of zircon crystals, in Rasbury, E.T., Hemming, S., and Riggs, N.,
1151 eds., *Mineralogical and Geochemical Approaches to Provenance: Geological Society of America
1152 Special Paper 487*, p. 13–36, doi: 10.1130 /2012 .2487 (02), 2012.
- 1153 Riggs, N.R., Reynolds, S.J., Lindner, P.J., Howell, E.R., Barth, A.P., Parker, W.G., and Walker, J.D.:
1154 The Early Mesozoic Cordilleran arc and Late Triassic paleotopography: The detrital record in
1155 Upper Triassic sedimentary successions on and off the Colorado Plateau: *Geosphere*, v. 9, p.
1156 602–613, 2013.
- 1157 Riggs, N.R., Oberling, Z.A., Howell, E.R., Parker, W.G., Barth, A.P., Cecil, M.R., and Martz, J.W.:
1158 Sources of volcanic detritus in the basal Chinle Formation, southwestern Laurentia, and
1159 implications for the Early Mesozoic magmatic arc: *Geosphere*, v. 12, p. 439–463, 2016.

- 1160 Saleeby, J., and Dunne, G.: Temporal and tectonic relations of early Mesozoic arc magmatism,
1161 southern Sierra Nevada, California, in Anderson, T.H., Didenko, A.N., Johnson, C.L., Khanchuk,
1162 A.I., and MacDonald, J.H., Jr., eds., Late Jurassic Margin of Laurasia—A Record of Faulting
1163 Accommodating Plate Rotation: Geological Society of America Special Paper 513, p. 223–268,
1164 2015.
- 1165 Saylor, J.E., and Sundell, K.E.: Quantifying comparison of large detrital geochronology data sets.
1166 *Geosphere*12, 203–220, 2016.
- 1167 Saylor, J.E., Jordan, J.C., Sundell, K.E., Wang, X., Wang, S., and Deng, T.: Topographic growth of
1168 the Jishi Shan and its impact on basin and hydrology evolution, NE Tibetan Plateau: *Basin*
1169 *Research*, v. 30(3), p. 544-563, 2018.
- 1170 Stewart, J.H., Anderson, T.H., Haxel, G.B., Silver, L.T., and Wright, J.E.: Late Triassic
1171 paleogeography of the southern Cordillera: The problem of a source for the voluminous
1172 volcanic detritus in the Chinle Formation of the Colorado Plateau region: *Geology*, v. 14, p. 567–
1173 570, 1986.
- 1174 Sundell, K.E., Saylor, J.E., and Pecha, M.: Sediment provenance and recycling of detrital zircons
1175 from Cenozoic Altiplano strata in southern Peru and implications for the crustal evolution of
1176 west-central South America: *Journal of South American Earth Sciences*, (in review), 2019.
- 1177 Surpless, K.D., Graham, S.A., Covault, J.A., and Wooden, J.L.: Does the Great Valley Group
1178 contain Jurassic strata? Reevaluation of the age and early evolution of a classic forearc basin:
1179 *Geology*, v. 34 (1), p. 21–24, 2006.
- 1180 Thomas, W.A., Gehrels, G.E., Greb, S.F., Nadon, G.C., Satkoski, A.M., and Romero, M.C.: Detrital
1181 zircon grains and sediment dispersal in the Appalachian foreland: *Geosphere*, v. 13 (6), p. 2206-
1182 2230, 2017.
- 1183 Thomas, W.A., Gehrels, G.E., Lawton, T., Satterfield, J., Romero, M., and Sundell, K.: Detrital
1184 zircon grains and sediment dispersal from the Coahuila terrane of northern Mexico into the
1185 Marathon foreland of the southern Midcontinent: *Geosphere*, v. 16 (in press), 2019.
- 1186 Tobisch, O.T., Fiske, R.S., Saleeby, J.B., Holt, E., and Sorensen, S.S.: Steep tilting of metavolcanic
1187 rocks by multiple mechanisms, central Sierra Nevada, California: *Geological Society of America*
1188 *Bulletin*, v. 112 (7), p. 1043–1058, 2000.
- 1189 Vermeesch, P.: Multi-sample comparison of detrital age distributions: *Chemical Geology*, v. 341,
1190 p. 140-146, 2013.
- 1191 Vermeesch, P.: Dissimilarity measures in detrital geochronology: *Earth-Science Reviews*, v.
1192 178: p. 310–321, 2018a. doi: 10.1016/j.earscirev.2017.11.027.
- 1193 Vermeesch, P.: Statistics for fission tracks. In Malus´a, M. and Fitzgerald, P., editors, *Fission*

- 1194 track thermochronology and its application to geology. Springer, 2018b.
- 1195 Wissink, G.K., Wilkinson, B.H., and Hoke, G.D.: Pairwise sample comparisons and
1196 multidimensional scaling of detrital zircon ages with examples from the North American
1197 platform, basin, and passive margin settings: *Lithosphere*, <https://doi.org/10.1130/L700.1>,
1198 2018.
- 1199 Woody, D.T.: Revised stratigraphy of the lower Chinle Formation (Upper Triassic) of Petrified
1200 Forest National Park, Arizona: *Museum of Northern Arizona Bulletin*, v. 62, p. 17–45, 2006.
- 1201 Wright, J.E., and Wyld, S.J.: Alternative tectonic model for Late Jurassic through Early
1202 Cretaceous evolution of the Great Valley Group, California, in Cloos, M., Carlson, W.D., Gilbert,
1203 M.C., Liou, J.G., and Sorensen, S.S., eds., *Convergent Margin Terranes and Associated Regions:
1204 A Tribute to W.G. Ernst: Geological Society of America Special Paper 419*, p. 1-15, 2007.
- 1205 Xie, X., Anthony, J.M., and Busbey, A.B.: Provenance of Permian Delaware Mountain Group,
1206 central and southern Delaware basin, and implications of sediment dispersal pathway near the
1207 southwestern terminus of Pangea: *International Geology Review*, DOI:
1208 10.1080/00206814.2018.1425925, 2018.

1209 **FIGURE CAPTIONS**

1210 **Figure 1.** Map showing the main basement provinces of southern North America and Mexico.
1211 Also shown are locations of the study area within the Colorado Plateau, outlines of Ancestral
1212 Rocky Mountains uplifts, and the Permian-Triassic magmatic arc along the continental margin
1213 of southwestern North America. Modified from Gehrels et al. (2011).

1214 **Figure 2.** Strata encountered in the Colorado Plateau Coring Project (adapted from Olsen et al.,
1215 2018). Sampled horizons are shown relative to core depth, stratigraphic depth, and
1216 stratigraphic nomenclature relevant for the Petrified Forest region. Detailed descriptions of
1217 samples are provided in DR Table 1; images of the sampled material are presented in Appendix
1218 1.

1219 **Figure 3.** Normalized probability density plots of U-Pb (zircon) ages from source terranes.
1220 Distinctive age groups include 1750-1620 Ma and 1520-1360 Ma ages from southwest Laurentia
1221 basement provinces, 1240-960 Ma ages from Grenville-age provinces exposed in the
1222 Appalachian and Ouachita orogens, 640-570 Ma and 480-370 Ma ages characteristic of the
1223 Appalachian orogen, 670-300 Ma ages from the Ouachita orogen, 300-260 Ma ages from the
1224 East Mexico arc, and 260-200 Ma ages belonging to the Cordilleran magmatic arc of
1225 southwestern North America. See text for sources of information.

1226 **Figure 4.** Plot showing the accuracy of $^{206}\text{Pb}^*/^{238}\text{U}$ dates of secondary standards analyzed
1227 during the current study. Each pair of symbols represents the weighted mean age and 2σ
1228 uncertainty of R33 and FC-1 analyses conducted with each sample, expressed as % offset from
1229 reported ID-TIMS dates of 1099.9 Ma for FC-1 (Paces and Miller, 1993) and 419.26 Ma for R33
1230 (Black et al., 2004). For FC-1, 1065 analyses are reported, with MSWD = 0.95 for all analyses. For
1231 R33, 295 analyses are reported, with MSWD = 0.92 for all analyses. Data are reported in DR
1232 Table 7.

1233 **Figure 5.** Normalized probability density plots of detrital zircon ages from our sample of the
1234 Coconino Sandstone and from other lower Permian sandstones of the Colorado Plateau.
1235 Numbers of constituent analyses are shown for each sample. Data are from ¹Dickinson and
1236 Gehrels (2003), ²Gehrels et al. (2011), ³Lawton et al. (2015), and ⁴this study. Shown for
1237 reference are age ranges from the Appalachian orogen (purple bands) and from local basement
1238 rocks (blue bands) (from Figure 3), which are interpreted by previous researchers to have
1239 sourced most of the detritus in these units. Also shown is our sample 383-2, which is
1240 interpreted to belong to the Wupatki Member of the Moenkopi Formation, but has an age
1241 signature characteristic of lower Permian strata of the Colorado Plateau.

1242 **Figure 6.** Probability density plots of detrital zircon ages from four samples from the Moenkopi
1243 Formation (lower four curves) as well as a Moenkopi sample from Dickinson and Gehrels
1244 (2008). Numbers of constituent analyses are shown for each sample. Samples 349-3, 335-1,
1245 327-2, and 319-2, plus the sample from Dickinson and Gehrels (2008), are all from the Holbrook

1246 Member. Sample 383-2 is interpreted to belong to the Wupatki Member, but has an age
1247 distribution that resembles lower Permian strata. Source regions are interpreted to include
1248 local basement rocks (blue bands), the Ouachita orogen (green bands), the East Mexico arc (red
1249 band), and the Late Permian-Triassic arc built along the Cordilleran margin (orange band).

1250 **Figure 7.** Normalized probability density plots of detrital zircon ages from twenty-four samples
1251 from the Mesa Redondo, Blue Mesa, Sonsela, and Petrified Forest Members of the Chinle
1252 Formation. Numbers of constituent analyses are shown for each sample. Age distributions older
1253 than 240 Ma are exaggerated by 10x. Tick marks indicate the preferred maximum depositional
1254 age for each sample (from DR Table 6). Source regions are interpreted to include local
1255 basement rocks (blue bands), the Ouachita orogen (green bands), the East Mexico arc (red
1256 band), and the Late Permian-Triassic arc built along the Cordilleran margin (orange band).
1257 Percent of all grains that are <240 Ma in age are shown for each sample on the left.

1258 **Figure 8.** Normalized probability density plots of detrital zircon ages from each set of samples
1259 analyzed in this study. Numbers of constituent analyses are shown for each sample. Age
1260 distributions older than 240 Ma for Chinle strata are exaggerated by 10x relative to <240 Ma
1261 ages. Age distributions for Moenkopi and Coconino Sandstones are exaggerated by 5x relative
1262 to Chinle ages. Source regions are interpreted to include local basement rocks (blue bands), the
1263 Ouachita orogen (green bands), the East Mexico arc (red band), and the Late Permian-Triassic
1264 arc built along the Cordilleran margin (orange band). Results from sample 383-2 are not
1265 included in this plot because of its uncertain stratigraphic position. Data from sample 131-2 are
1266 omitted because they differ from ages present in other samples from the Petrified Forest
1267 Member. Percent of all grains that are <240 Ma in age are shown for each sample on the left.

1268 **Figure 9.** MDS plot comparing age distributions of samples analyzed herein with each other and
1269 with possible source areas. MDS (metric) analyses are based on the cross-correlation
1270 coefficient, and were conducted using the software of Saylor et al. (2018). Data from samples
1271 analyzed herein are in DR Table 3. Ages for source regions are from the sources cited in the
1272 text. Stars represent MDS values for sets of examples, with the exception that sample 131 is not
1273 included with other Petrified Forest samples."

1274 **Figure 10.** Density distributions of U concentration versus U/Th for Triassic grains in the four
1275 chronostratigraphic units recognized in this study. Plots made with Hf density plotter software
1276 of Sundell et al. (2019).

1277 **Figure 11.** MDS plot comparing age distributions of Permian strata of the Colorado Plateau with
1278 each other and with potential source regions including the Appalachian orogen, Ouachita
1279 orogen, and basement rocks of southwestern North America. Data sources are described in
1280 Figures 3 and 4. The data support the interpretation of Lawton et al. (2015) that the Coconino,
1281 Cedar Mesa, and White Rim sandstones (cool shades) belong to a regional blanket of eolian
1282 strata that was derived largely from the Appalachian and/or Ouachita orogen, where strata of

1283 the Castle Valley and Cutler formations (warm shades) include greater proportions of detritus
1284 derived from local basement sources.

1285 **Figure 12.** Sketch map of relevant tectonic features in southwestern Laurentia during Late
1286 Triassic time [adapted from Figure 42 of Dickinson (2018)].

1287 **Figure 13.** Plot showing interpreted maximum depositional ages (and 2σ uncertainties) for each
1288 sample, as determined by the four methods described above and reported in DR Table 6.
1289 Preferred ages (vertical red lines) are the average of the ages calculated by these four methods.
1290 CA-TIMS and ID-TIMS ages are shown in approximate stratigraphic position (as shown by Kent
1291 et al., 2019), with outcrop samples in gray symbols and core samples using black symbols.
1292 Smaller symbols represent ID-TIMS ages or CA-TIMS ages based on a single age or of uncertain
1293 reliability. Stratigraphic units are keyed to dominant rock type, with brown = mudstone and
1294 siltstone, yellow = sandstone, pink = bentonite. Average grain size of each sample is shown with
1295 bars on left (from Appendix 1 and DR Table 1). PDP curves to right show 2.0 Ga to 240 Ma ages,
1296 as plotted on Figure 7. Also shown are age models of Kent et al. (2019) and Rasmussen et al.
1297 (2020). Vertical red bands show interpreted ages of main clusters of maximum depositional
1298 ages.

1299 Curves across top of diagram show the distribution of ages from (1) fore-arc strata of the
1300 Barranca and El Antimonio Groups in Sonora (Gonzalez-Leon et al., 2009; Gehrels and Pecha,
1301 2014) and the Great Valley Group in California (DeGraaff-Surpless et al., 2002; Surpless et al.,
1302 2006; Wright and Wyld, 2007), (2) Permian-Triassic igneous rocks in California (Chen and
1303 Moore, 2002; Miller et al., 1995; Tobisch et al., 2000; Barth and Wooden, 2006, 2011, 2013;
1304 Saleeby and Dunne, 2015), and (3) strata of the Chinle Formation in other parts of the Colorado
1305 Plateau (Dickinson and Gehrels, 2008; Riggs et al., 2012; Marsh et al., 2019). Diamond-shaped
1306 symbols beneath curves represent individual ages.

1307 **Figure 14.** Depositional model of strata of the Chinle Formation encountered in the CPCP core.
1308 Each time slice contains information about the dominant grain size of the host sedimentary
1309 rock, the abundance of syn-depositional-age zircon grains that are interpreted to be air-fall in
1310 origin, and the abundance of recycled zircon grains that pre-date deposition.

Figure 1 (NAmap)

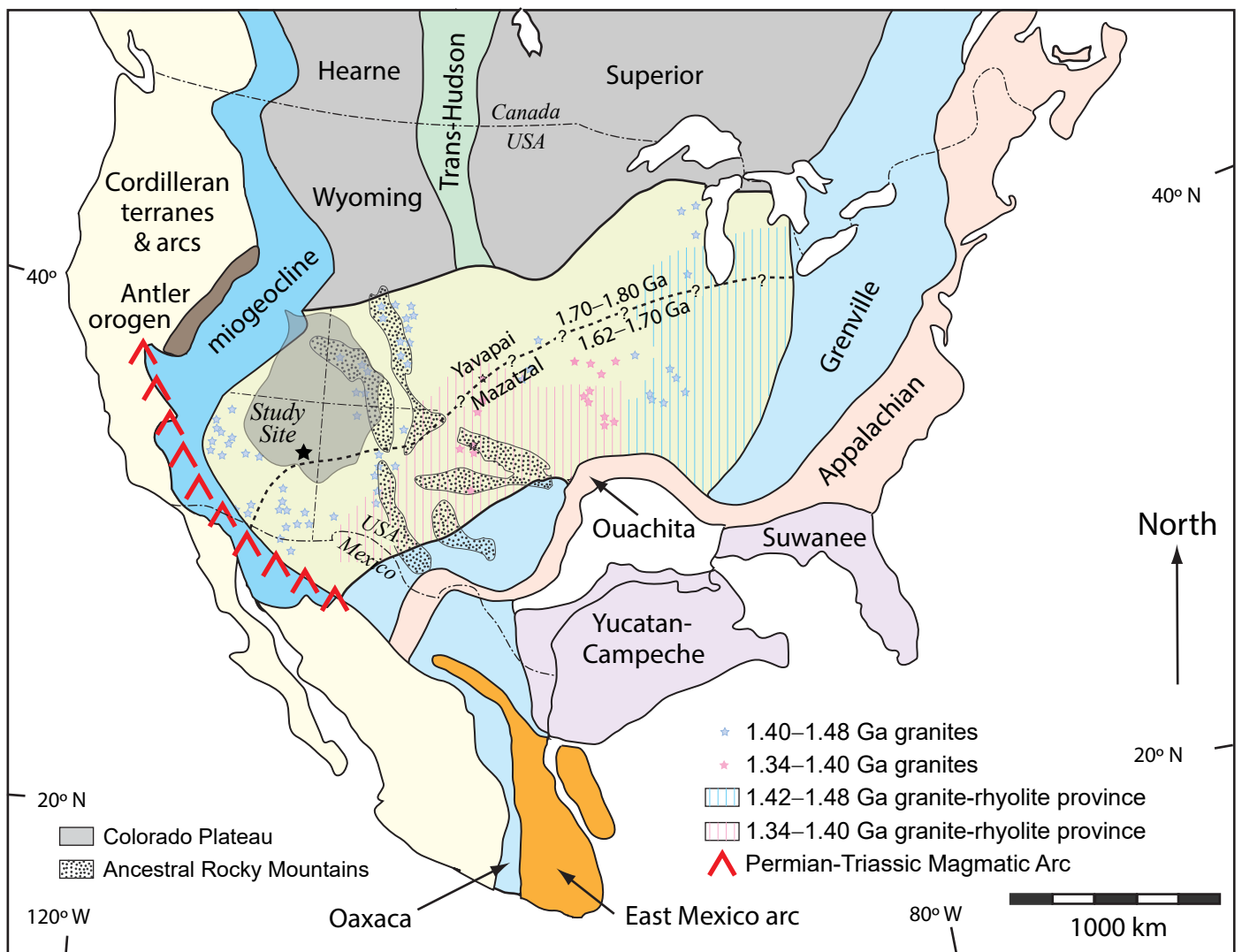


Figure 2 (Strat Column)

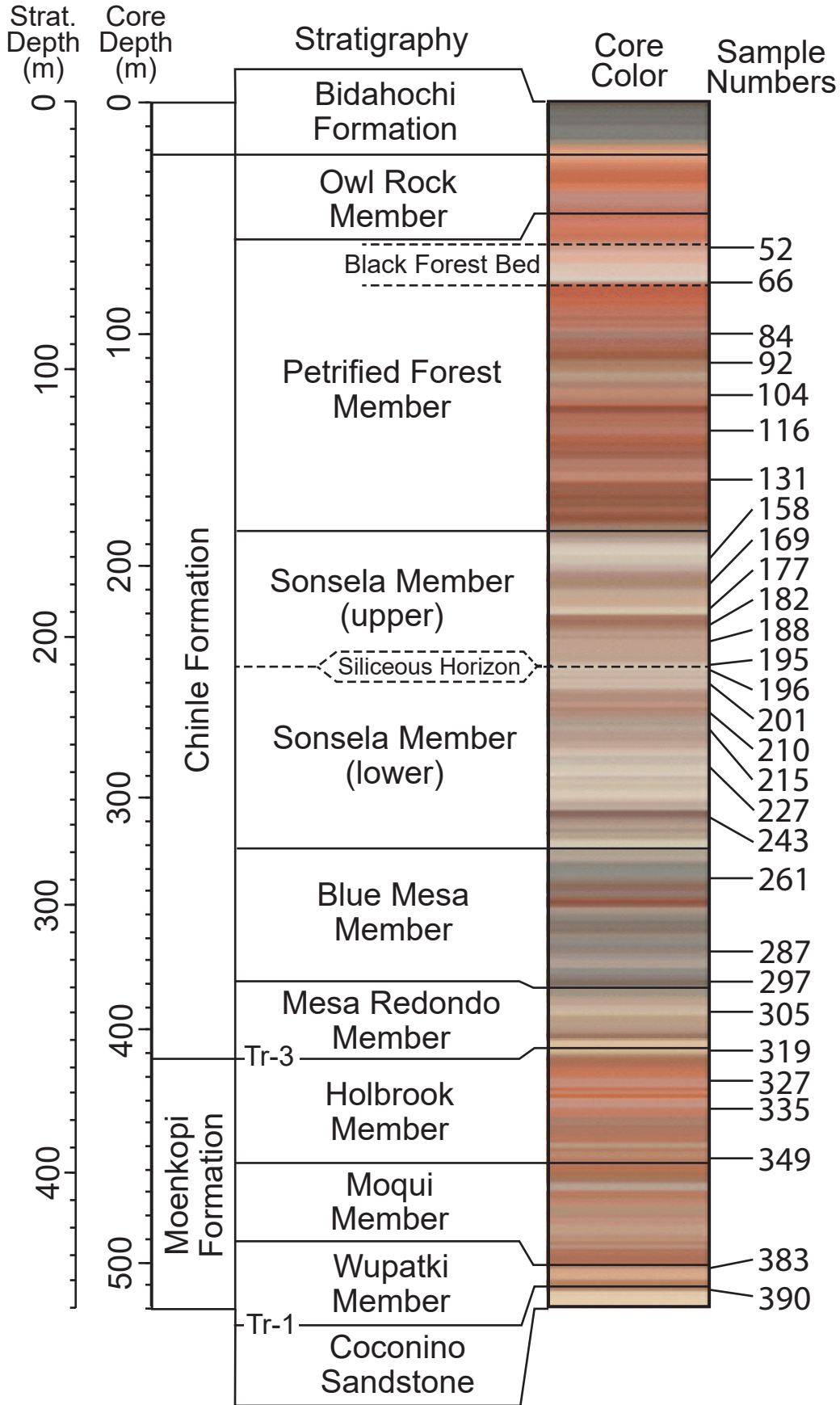


Figure 3 (App-Ouach-Bsmt-EMArc-CordArc PDP)

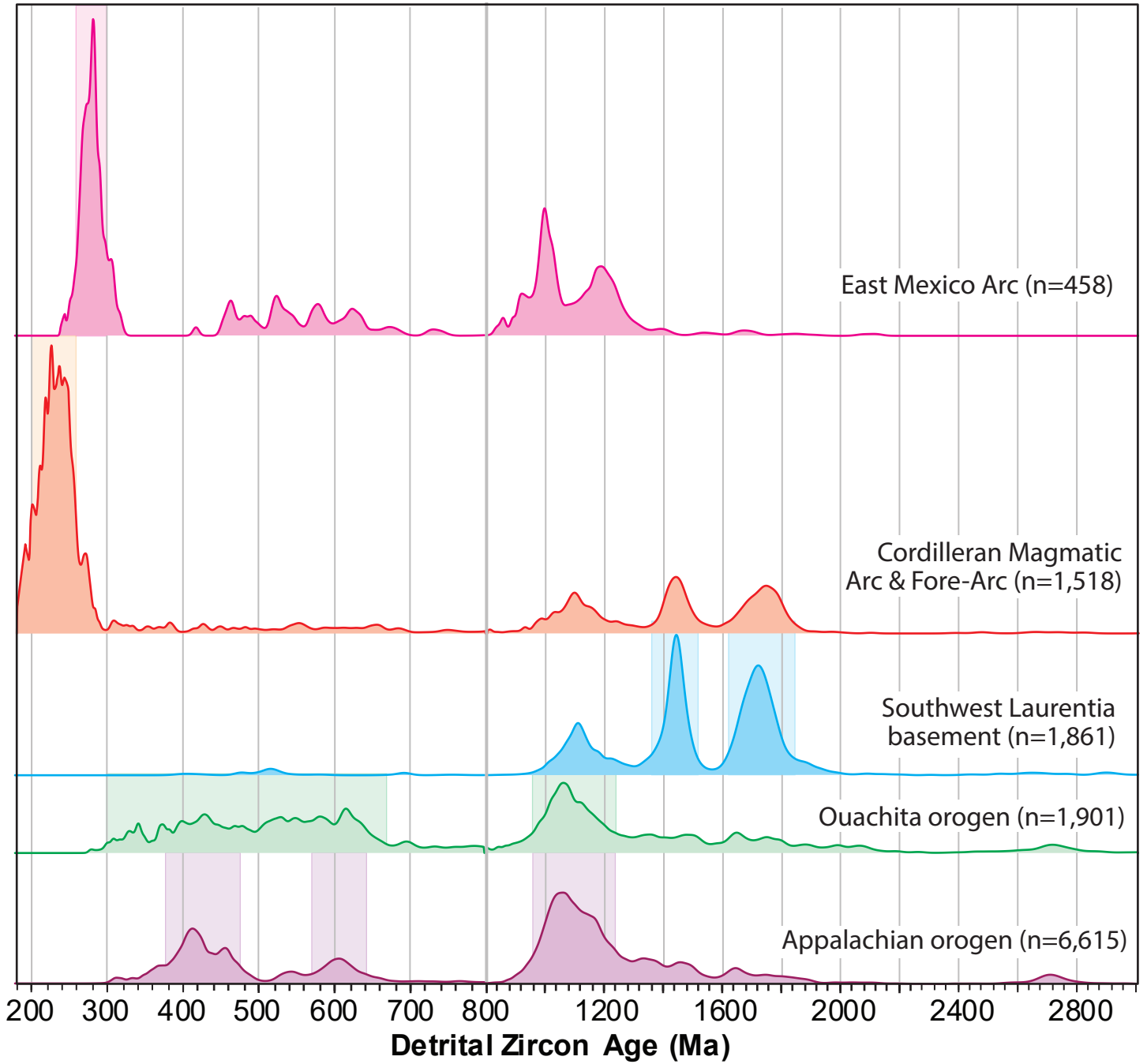


Figure 4 (Standard Ages)

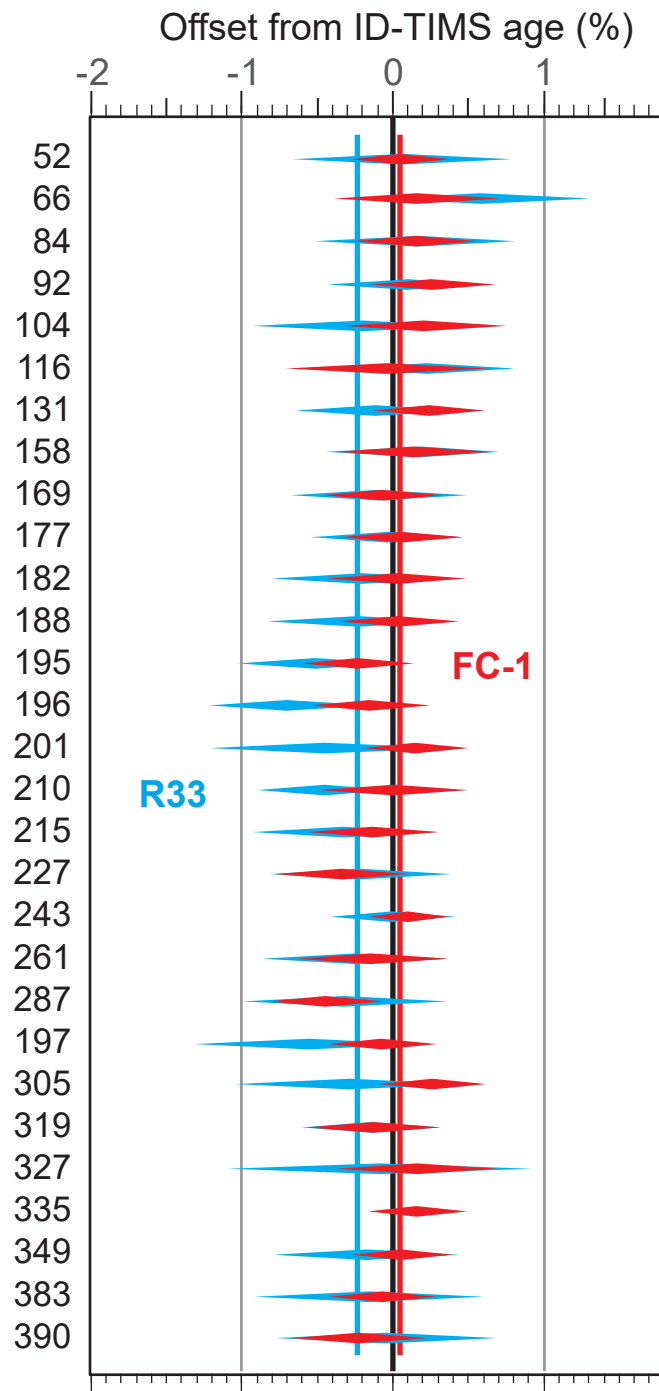


Figure 5 (Coconino PDP)

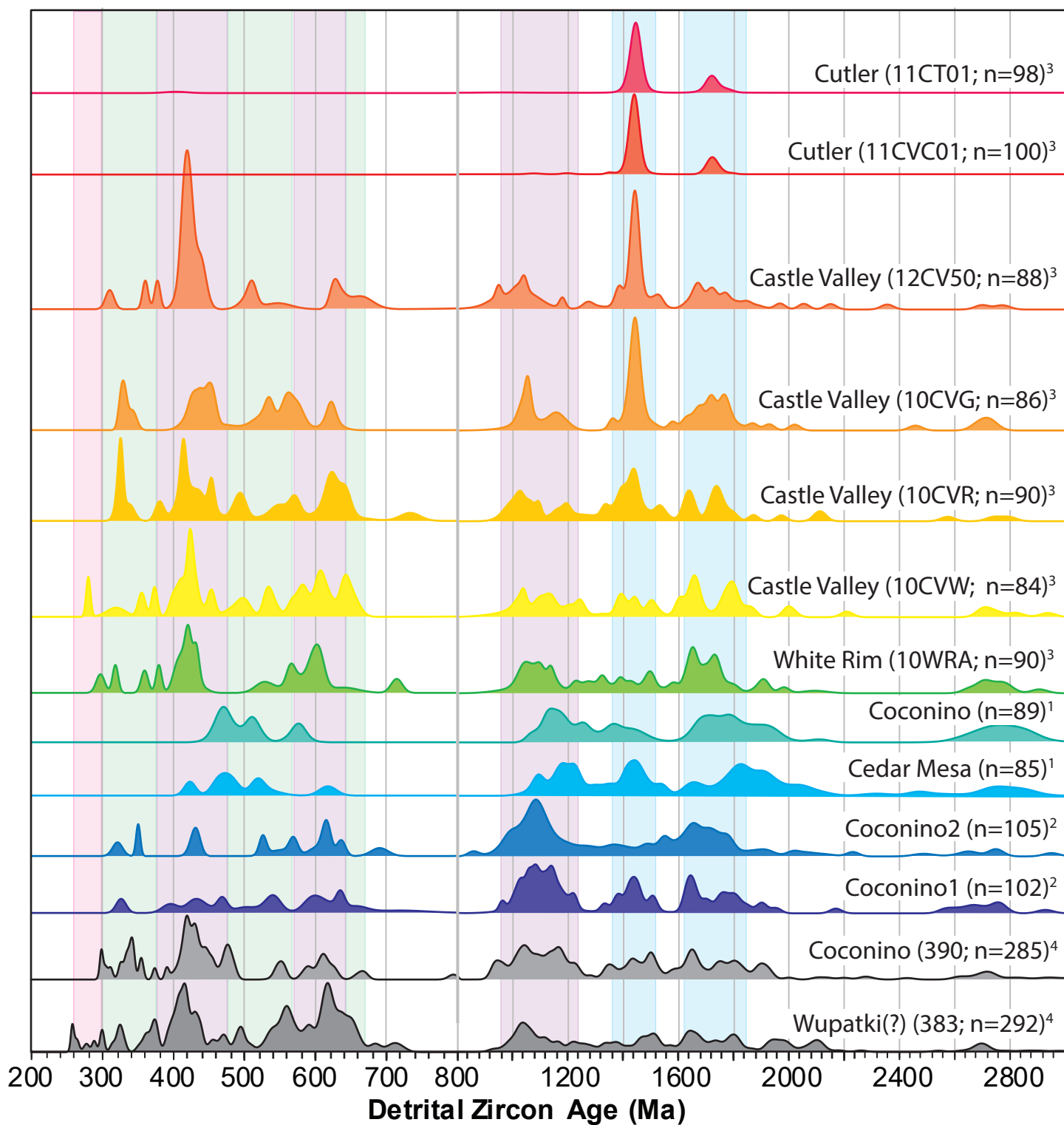


Figure 6 (Moenkopi PDP)

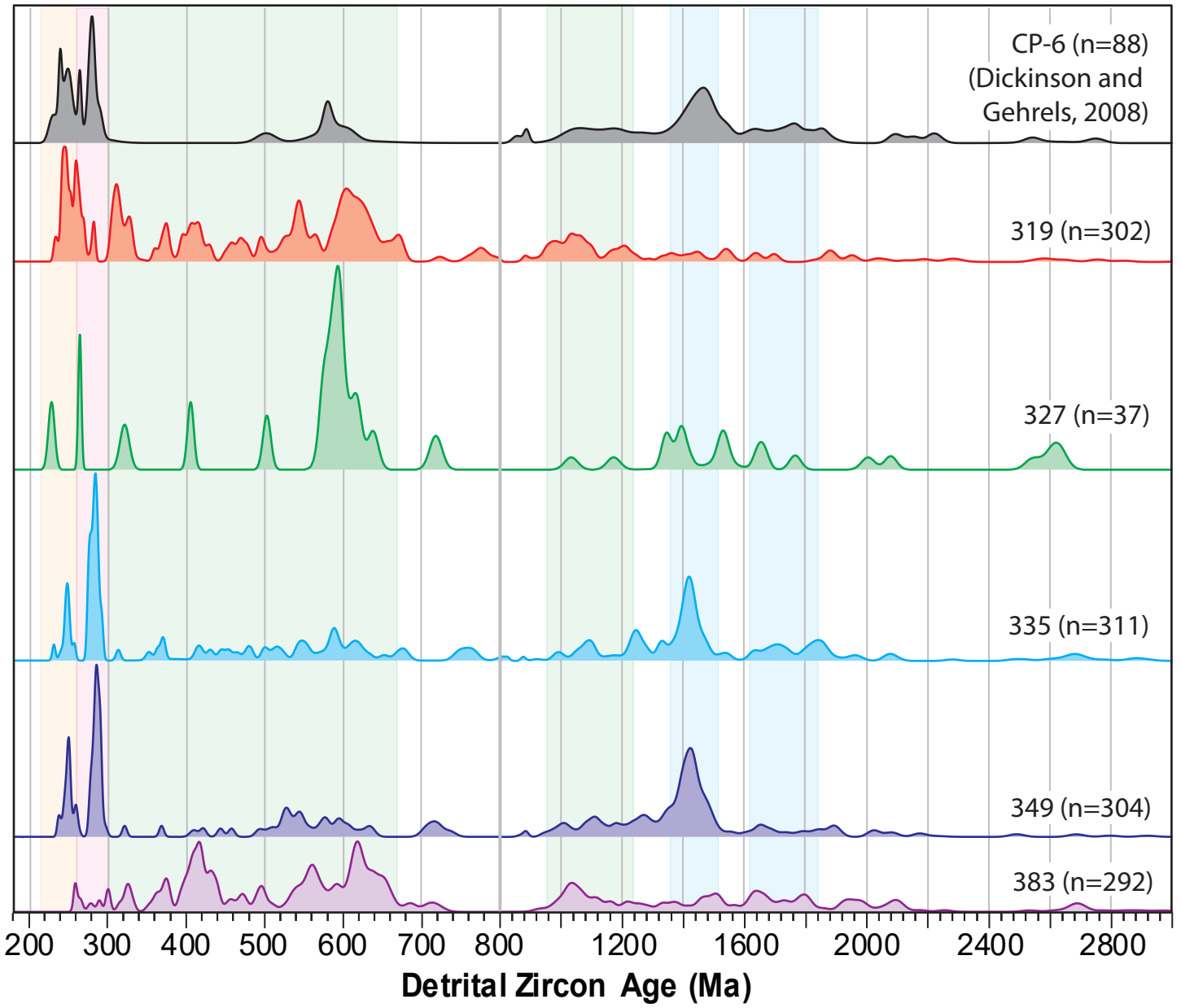


Figure 7 (Chinle PDP)

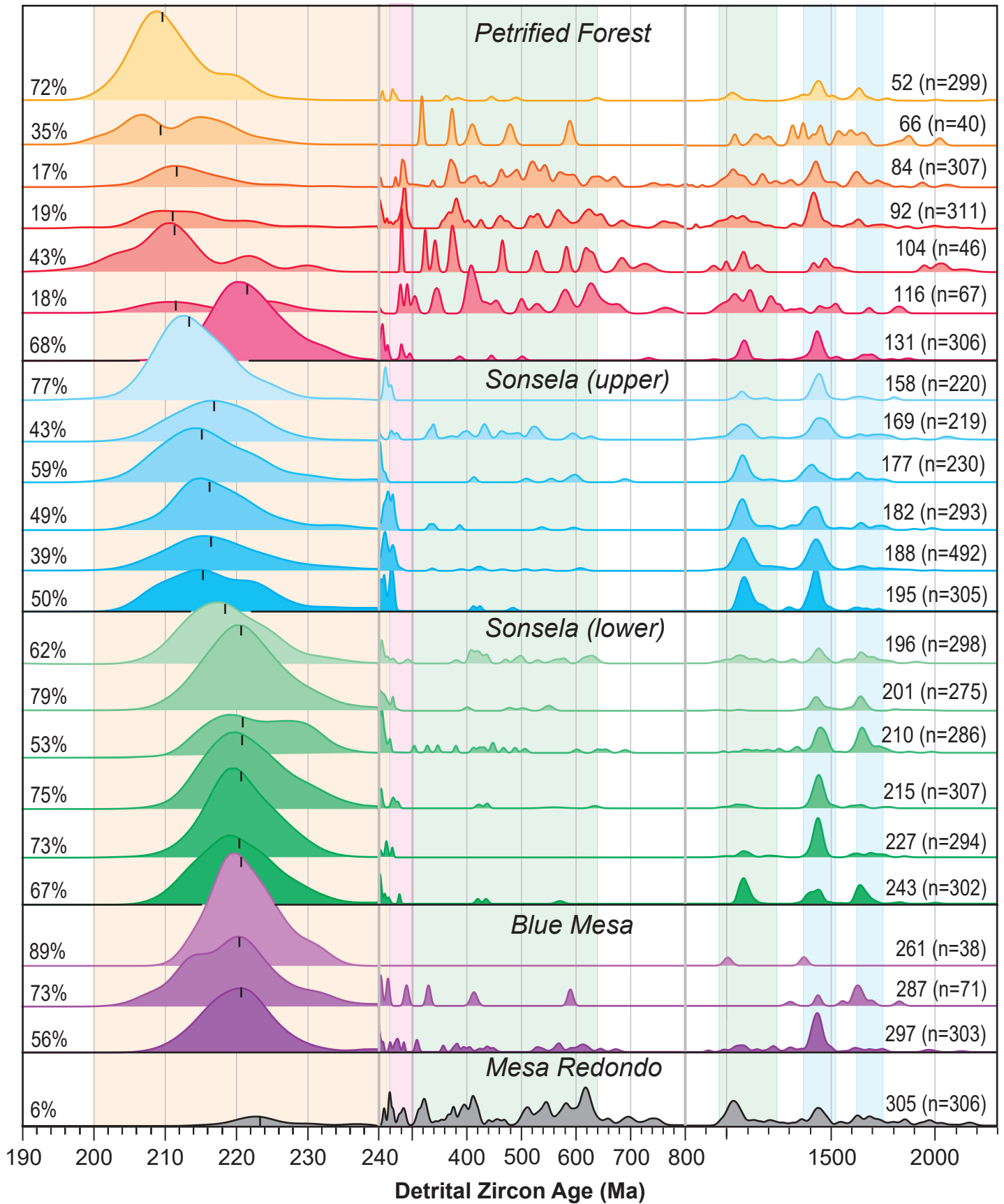


Figure 8 (Coco-Moen-Chin PDP)

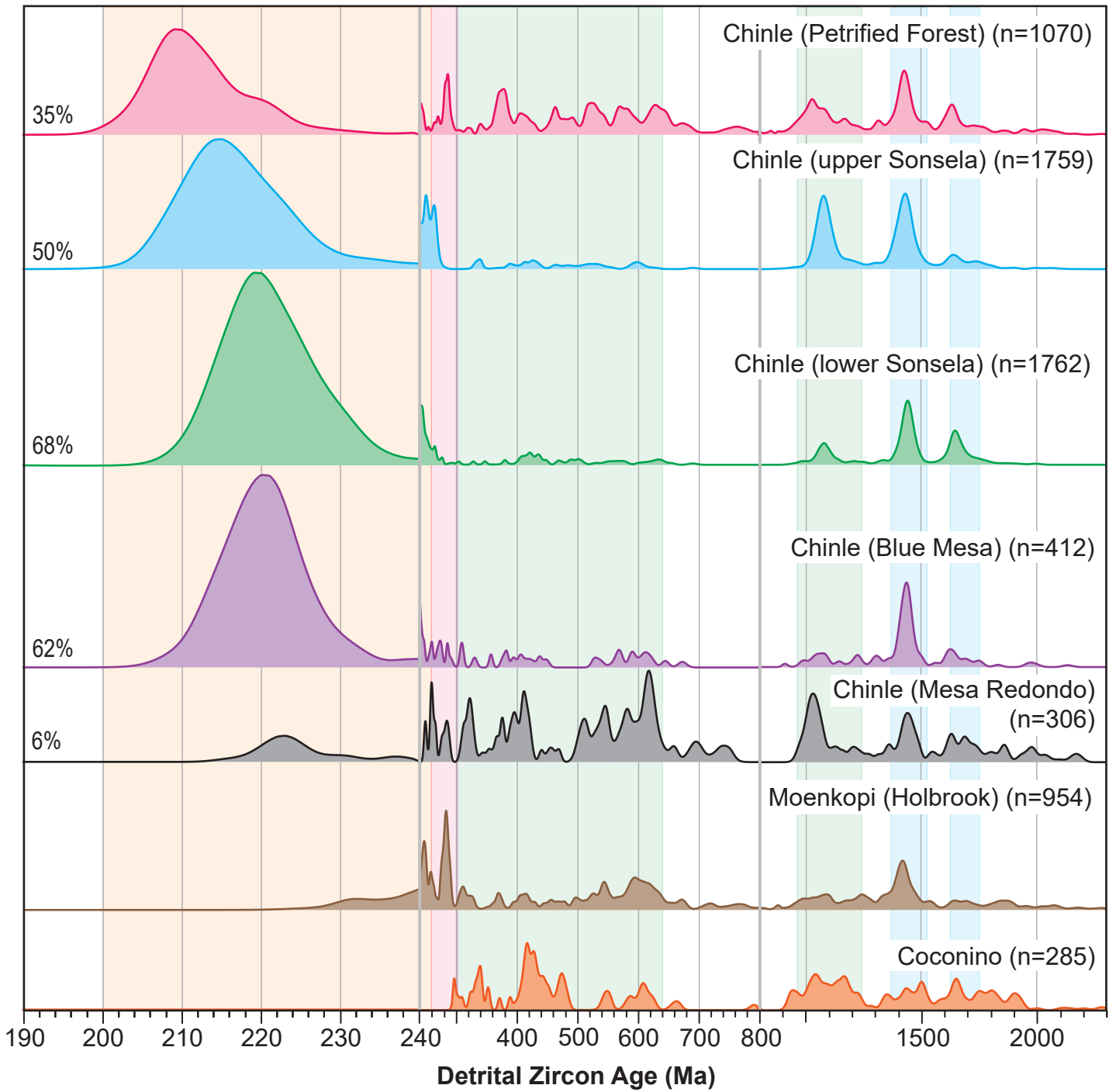


Figure 9 (MDS Plots)

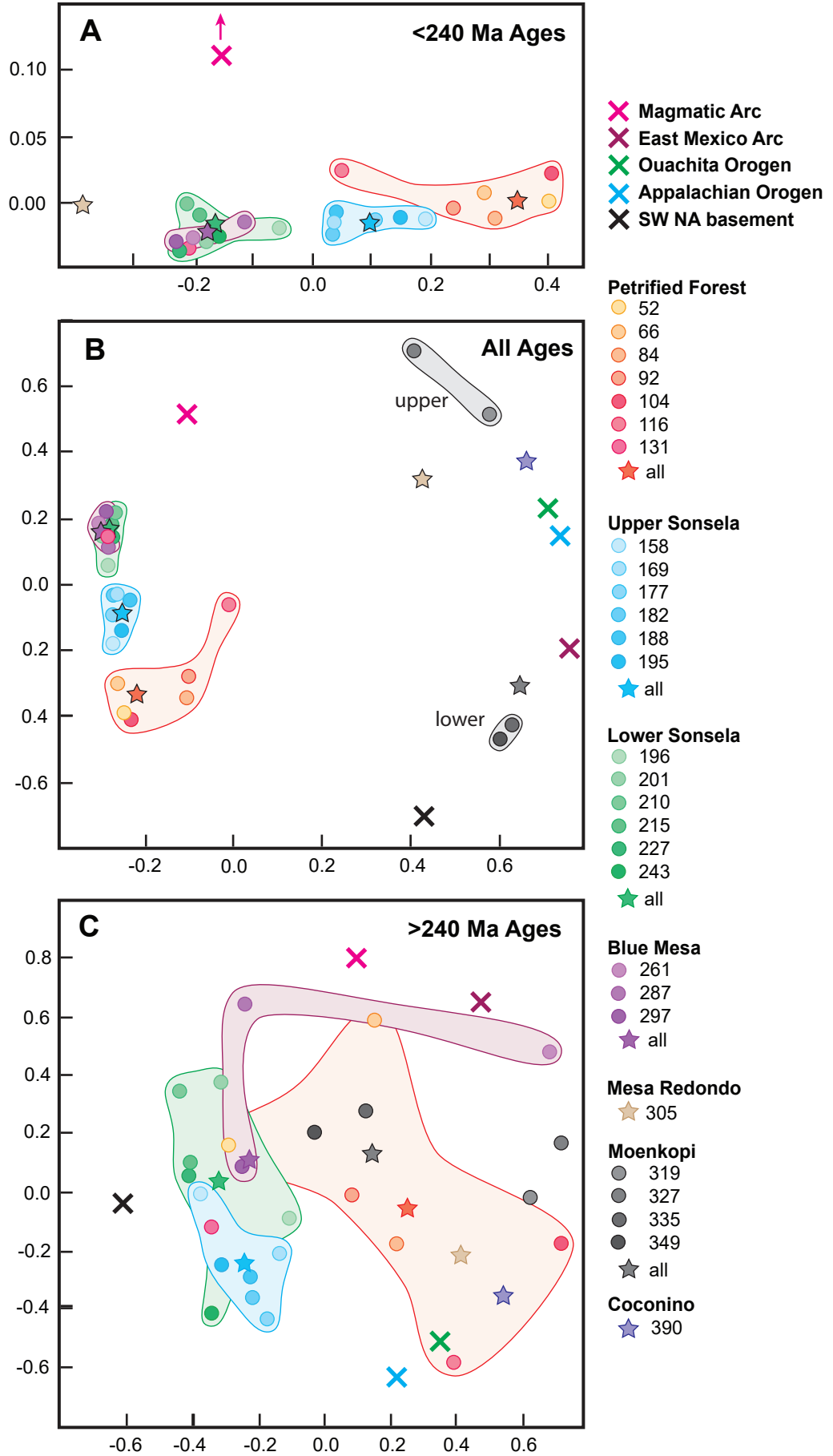


Figure 10 (Uconc-UTh plot)

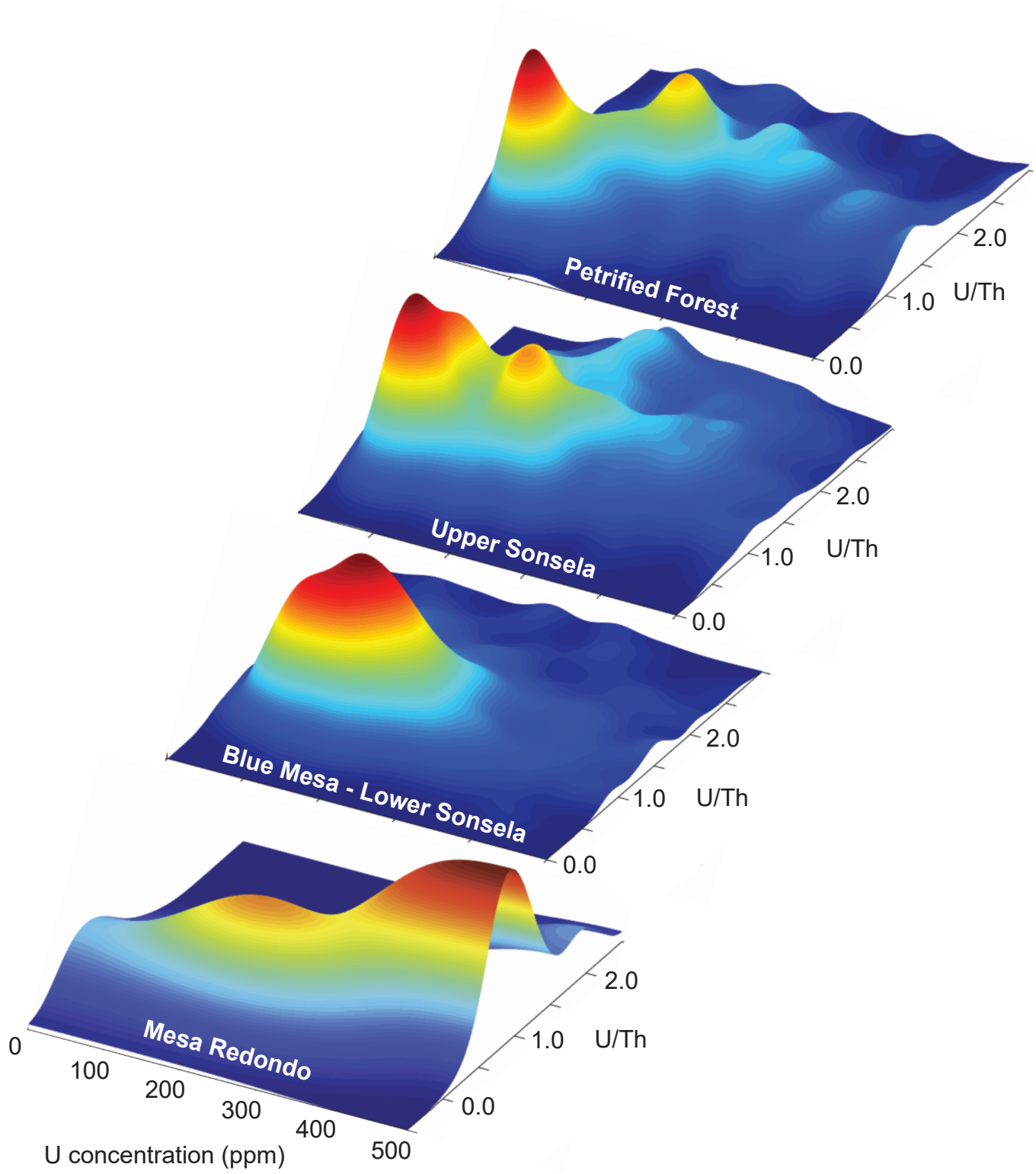


Figure 11 (AOB CO MDS plot)

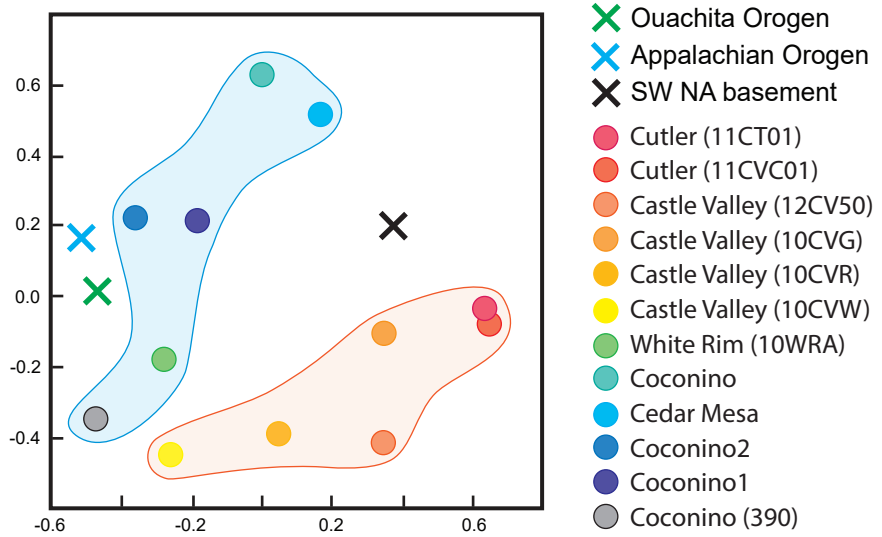


Figure 12 (Triassic Paleogeography)

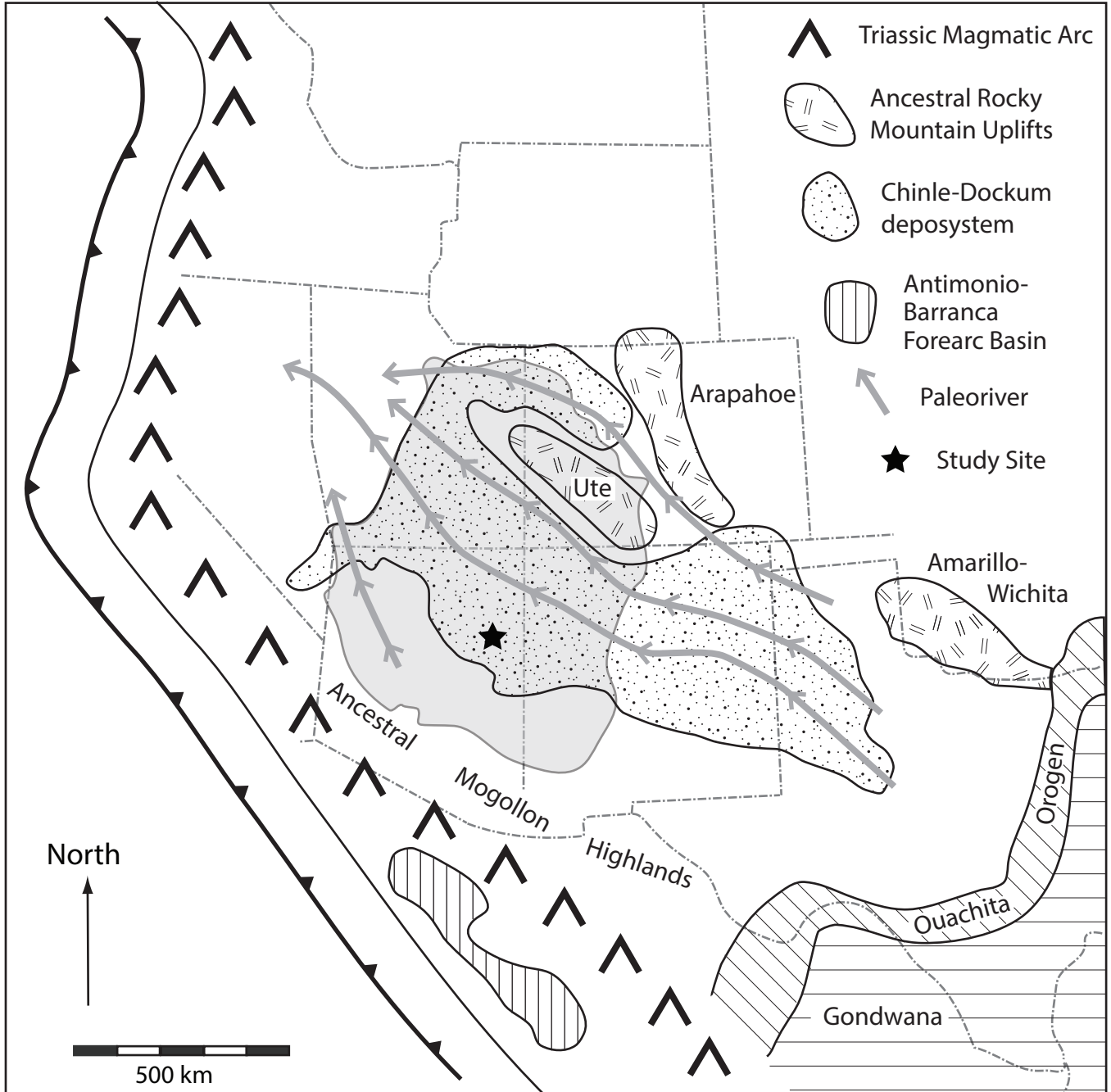


Figure 13 (DZ MDA plot)

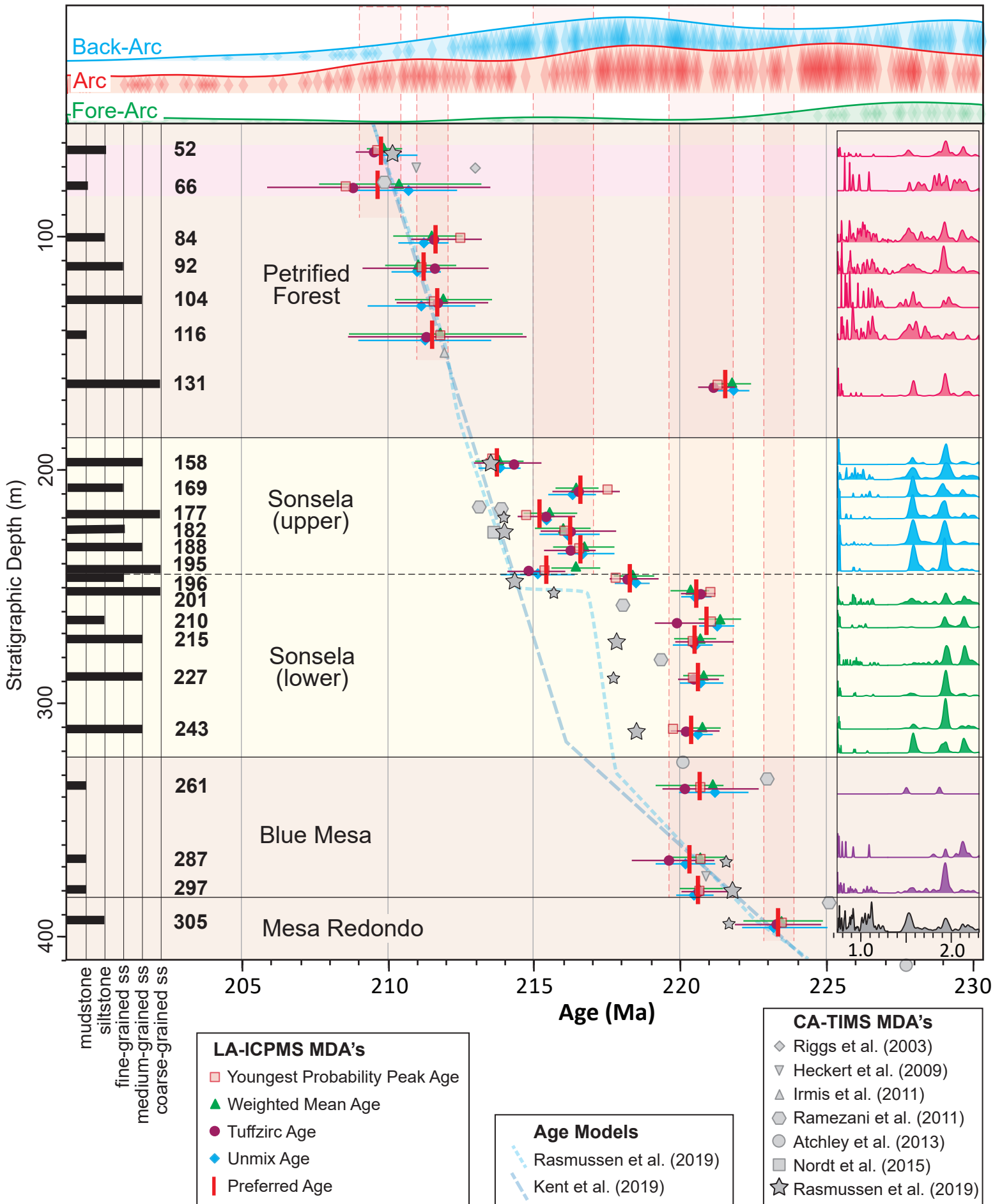
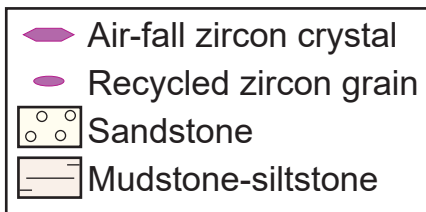
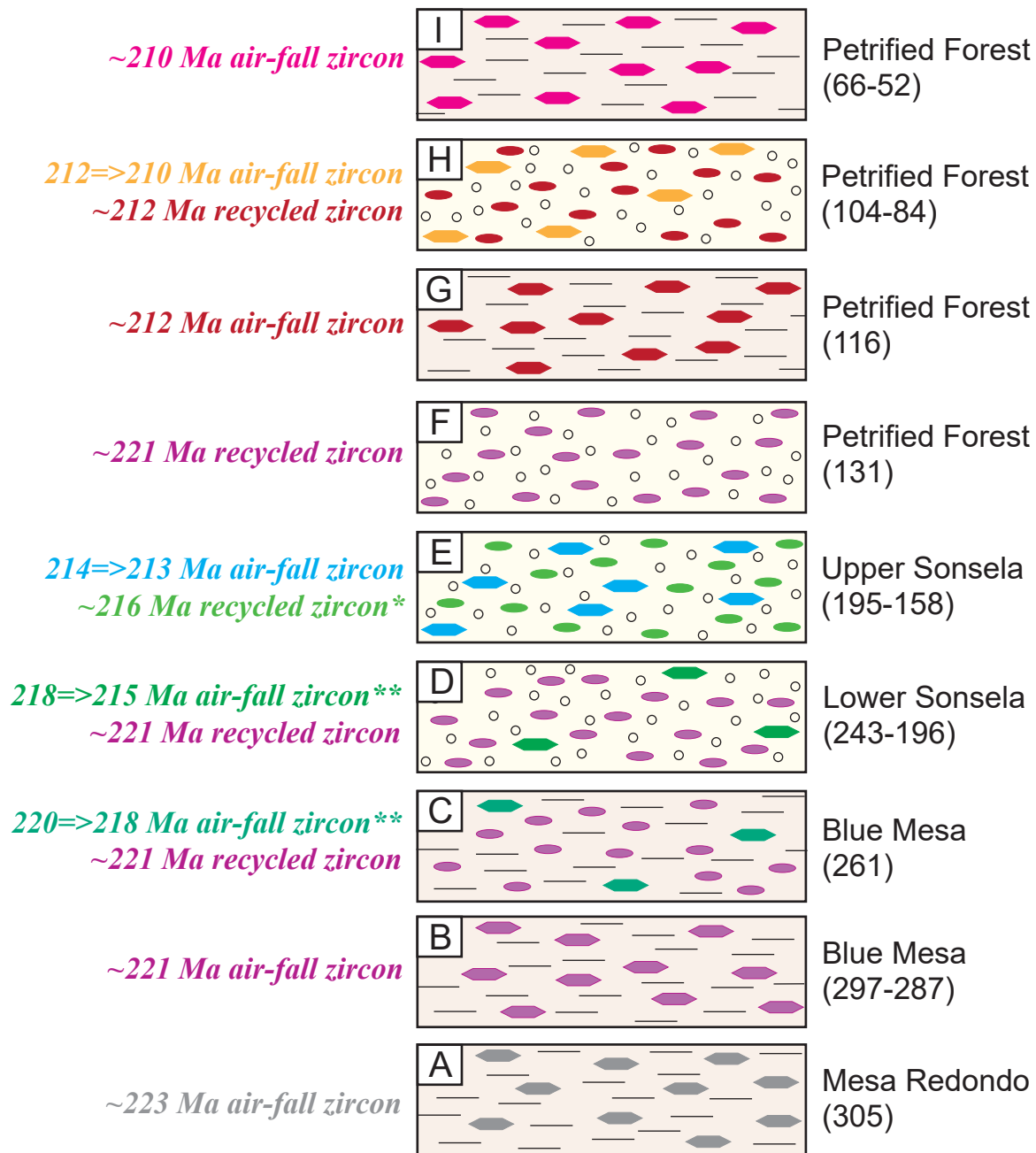


Figure 14 (Chinle Strat)



**Uncertain source for ~216 Ma recycled grains in upper Sonsela*

***Low abundance of 220-215 Ma air-fall grains in lower Sonsela*

Appendix 2 (CA-TIMS vs LA-ICPMS ages)

